Pyrolysis of Phenolic Resin and Carbon/Phenolic Composites

by

Celeste H. A. Guiles

B.S., University of Hawaii, 2021

A thesis submitted to the

Faculty of the Graduate School of the

University of Colorado in partial fulfillment

of the requirement for the degree of

Doctor of Philosophy

Ann & H.J. Smead Department of Aerospace Engineering Sciences

2025

Committee Members:

Timothy K. Minton, Chair

Francisco Lopez Jimenez

Hisham Ali

Barney Ellison

Alexandre Martin

Guiles, Celeste Hi‘ilani Anthea (Ph.D., Aerospace Engineering [Ann & H.J. Smead Department of Aerospace Engineering Sciences])

Pyrolysis of Phenolic Resin and Carbon/Phenolic Composites

Thesis directed by Professor Timothy K. Minton

Quantification of gaseous products formed during the pyrolysis of ablative heat shield materials is essential for understanding the decomposition mechanism of these materials and can provide a foundation to develop improved materials response models. For this purpose, an experimental setup based on previous work has been assembled and calibrated, a data analysis method has been developed, and experimental campaigns have been conducted on three different materials relevant to atmospheric entry heat shields: pure SC-1008 phenolic resin, phenolic-impregnated carbon ablator domestic (PICA-D), and three-dimensional mid-density carbon phenolic insulation layer (3MDCP-IL). Product yields were derived from mass spectra of volatile pyrolysis products, collected as a function of sample temperature over the range of 25-1200 °C at five linear temperature gradients with respect to time, in the range of ~1 – 25 °C s^{-1}. Normalized molar and mass yields for each pyrolysis product and temperature gradient have been measured for each material, and thermogravimetric analysis curves have been synthesized from the temperature-dependent mass yield data and measurements of total mass loss. The data were used in conjunction with data in the literature to identify the temperature-dependent pyrolysis mechanisms for each material and identify the effects of temperature gradient, density, temperature nonuniformity, curing procedures, and carbon fibers.

Dedication

To my dad, Dr. Martin Guiles, for being my inspiration and someone I deeply admired.

Acknowledgements

Thank you to my family and friends for supporting me through this journey. Thank you to my two adorable kitties Noodle and Lily for being there for me when I come home from the lab. I want to thank all of my teachers and mentors throughout the years, and especially Dr. Matthew Cain, Dr. Kathleen Ogata, and Dr. Radovan Milincic, who helped my enthusiasm for science grow, and gave me opportunities to engage with the scientific community. Thank you to all the colleagues I have had throughout graduate school, Chenbiao, Samer, Aki, Pedro, Brian, Chandan, Yanice, Lidia, Cameron, Cornelia, Adriana, Megan, Gavin, and Irina. And a special thank you to my advisor, Professor Timothy Minton, for giving me so many opportunities and helping guide me through my Ph.D. work. I would like to thank Dr. Brody Bessire for paving the way for my research, and for helping supply samples and always being available for discussions. I would like to thank all my collaborators, and especially Jeff Engerer and Bernadett Hernandez-Sanchez at Sandia, and Alexandre Martin and Savio Poovathingal at the University of Kentucky. Finally, thank you to NASA and Sandia National Labs for funding my work.

Table of Contents

List of Tables

List of Figures

Chapter 1

Introduction

Space vehicles that enter a planetary atmosphere experience extreme temperatures as kinetic energy is quickly decreased. The kinetic energy associated with the high-speed flow relative to the vehicle is abruptly converted to internal energy through a shockwave, leading to high temperature (~10^4 K) gas in the shock layer.[1] The hot gas transfers heat to the vehicle surface; thus, a thermal protection system (TPS) is required to shield the vehicle and its internal components. Ablative TPSs, used for entry and re-entry purposes, protect the vehicle from extreme temperatures by absorbing heat inside the TPS through endothermic pyrolysis reactions and by attenuating the heat flux before it reaches the TPS through the blowing of pyrolysis gases into the incoming flow. Ablative TPS materials are commonly made from carbon phenolic composites.[2] For example, PICA (phenolic impregnated carbon ablator), a lightweight TPS material used on missions such as Mars Science Lab and Mars 2020, is a composite of the phenolic derived by curing Durite™ SC-1008 resole resin and a rigid carbon fiber preform (FiberForm, Fiber Materials Inc., Biddeford, ME).[3] Some applications use denser carbon phenolic materials made of layered phenolic impregnated carbon fabric.[2] The thermal response of these heat shield materials is influenced by the internal pyrolysis reactions as the phenolic resin pyrolyzes, chars, and ablates. Accurate material response models are necessary to optimize the material, shape, and thickness for specific entry, decent, and landing scenarios.[4] Because discrepancies are seen between current state-of-the-art model predictions and flight data, a better understanding of the thermal decomposition mechanisms of phenolic resin in TPS materials would be expected to lead to

improved material response predictions and guide the design and use of TPSs for future missions.[2,4,5]

Many studies have been performed on the pyrolysis of pure phenolic resin and phenolic-based ablative heat shields, with the main experimental methods being infrared (IR) spectroscopy, gas chromatography with mass spectrometry (GC-MS), and thermogravimetric analysis (TGA). IR spectroscopy can identify certain functional groups and therefore can characterize changes in bonding as phenolic resin is heated and charred. This method is useful for inferring decomposition mechanisms; however, it cannot identify or quantify gaseous products. GC-MS can precisely identify and quantify products; however, the use of this method usually requires trapping of pyrolysis gases and subsequent re-heating before measurement, which may introduce secondary reactions. Neither IR spectroscopy nor GC-MS methods allow for the continuous monitoring of the material as it transforms from a pristine material to a carbon char, making it difficult to unravel the pyrolysis pathways at TPS-relevant temperature gradients. TGA provides accurate in situ measurements of mass loss as the resin is pyrolyzed, but coupling with another system, such as a mass spectrometer, is required to detect products, and the detection of product molecules generally occurs after they have passed through a sampling tube and have undergone many potentially reactive collisions. Such a sampling arrangement also makes it difficult to quantify the flux of primary pyrolysis products that leave the heated sample. TGA is also limited to relatively low temperature ramps with respect to time, which are needed to minimize thermal gradients and temperature lag.

The experimental approach used for the study described herein is complementary to IR spectroscopy and overcomes some of the limitations of GC-MS and TGA. This approach uses molecular beam sampling coupled with a mass spectrometer and is a variant of a technique often

referred to as molecular beam mass spectrometry (MBMS). MBMS has been effectively used in studies of combustion chemistry,[6,7] where gaseous products from a combustion source at pressures up to 760 Torr are sampled and collimated with two skimmers across two regions of differential pumping, forming a collisionless flow (molecular beam) which is directed into the ion source of a time-of-flight or quadrupole mass spectrometer. Thus, MBMS allows primary gas-phase reaction products to be detected in situ from the relatively high-pressure region where they are produced. The mass spectrometer typically detects number density, but the flux of products entering the ionization region may be determined if their velocities in the molecular beam are known. In our implementation of MBMS, the gaseous products from a pyrolyzing material are collimated through two apertures separating differentially-pumped detected in an essentially collisionless stream that follows a direct path in vacuum from the heated sample to an electron impact quadrupole mass spectrometer. With this approach, the fluxes of primary products may be measured directly, without any collisions, after they leave the sample. Samples are small and heated from all sides, minimizing thermal gradients and allowing for high linear temperature gradients with respect to time (referred to in this paper simply as “temperature gradients”). As the detection method is only sensitive to primary gaseous products, IR spectroscopy studies provide important complementary information about the remaining material when inferring the thermal decomposition mechanisms. The new results reported herein have been interpreted in light of two prior studies in our laboratory, which used a similar heating and in situ detection method. These prior studies focused on molar and mass yields of the gases evolved during the pyrolysis of PICA.[8,9] Subsequent to these earlier studies, several changes were made to the apparatus and experimental protocol to ensure increased accuracy in temperature measurements and yield determinations. Key changes in the experiment include omnidirectional sample heating, improved determination of sample temperature,

collimation of the beam for accurate flux measurements, and a high-sensitivity mass spectrometry detection system.

The this first study that was conducted with the updated system was to investigate the pyrolysis of pure SC-1008 phenolic resin by obtaining high-fidelity molar and mass yields as a function of temperature and temperature gradient. Such data may be used as a benchmark for the interpretation of pyrolysis data on carbon-phenolic composites and thereby give greater insight into the decomposition mechanisms and kinetic rates of the relevant thermal decomposition reactions, ultimately improving material response models for TPSs and reducing discrepancies between predictions and flight data. The study of the pure phenolic resin used in composite heat shields is beneficial before exploring the carbon-phenolic composites for two main reasons: (1) it removes the effect of the carbon phase, e.g., reactions of pyrolysis gases or the resin phase with carbon fibers, and (2) the samples are not proprietary and can be prepared, stored, and studied under controlled laboratory conditions. Additionally, detailed high fidelity studies of quantitative pyrolysis products of SC-1008 at different temperature gradients have not been conducted before.

The second study conducted was on the pyrolysis of PICA-D (phenolic impregnated carbon ablator – domestic). PICA-D is a new ablative heat shield that will replace PICA, and will be used on NASA's Dragonfly mission. PICA-D is a carbon-phenolic composite composed of chopped lyocell derived carbon fibers (which is domestically sourced) and impregnated with SC-1008 resin. The study of this material is beneficial as it is a real engineering material that needs to be modeled, and because its temperature dependent and temperature gradient dependent decomposition mechanism has not been studied before.

The third study was on 3MDCP-IL (3D medium density carbon phenolic – insulation layer), a type of woven heat shield that may be used on NASA's Mars Sample Return mission.

This material is composed of woven polyacrylonitrile (PAN) derived carbon fibers, woven Kynol novalak based phenolic resin fibers, and impregnated with SC-1008 resin. The benefits of studying this material are the same as studying PICA-D, as it is a real engineering material that needs to be models, and its temperature dependent and temperature gradient dependent decomposition mechanism has not been studied before.

For each study of the three materials, five temperature gradients were chosen, which span those measured at various positions on the Mars Science Laboratory PICA heat shield[10] (approximately 1 – 25 °C s^{-1}) with four of these temperature gradients being similar to those used in one of the previous studies in our laboratory.[8] The temperature gradients observed in the flight data are not linear because of turbulence and other variables; however, linear temperature gradients were used during the experiments to avoid extra complexity. Pyrolysis gases with masses between 0.5 and 200 Da were detected in situ as the resin was heated at each of the five temperature gradients. Molar and mass yields of gaseous products were determined as a function of sample temperature, and synthesized TGA curves were also calculated from the mass yield data and measurements of total mass loss. All studies were used, in conjunction with each other and related work, to obtain further insight into the nonequilibrium thermal decomposition mechanisms of phenolic resin and carbon-phenolic composites and set a benchmark for future studies.

Chapter 2

Experimental Methods

All three studies described in this thesis were performed on the pyrolysis apparatus that was updated based on comments and concerns regarding the fidelity of the previous pyrolysis experiments performed by Bessire and Minton.[8,9] This apparatus can be used for the pyrolysis of all types of materials, however the data analysis method is currently set up to only handle phenolic resin based materials.

2.1 Experimental Configuration for Pyrolysis 2.0

The experimental apparatus (**Figure 2.1a**) is a high vacuum system with an in situ Extrel research-grade electron-impact quadrupole mass spectrometer with 19 mm rods. The source and differential chambers are pumped by Pfeiffer turbomolecular pumps (TMH 1601 P and TMH 521 P, respectively), and the detector chamber is pumped with an Edwards nEXT 400 model turbomolecular pump. The source chamber has a base pressure of 10^{-7} Torr; the differential chamber has a base pressure of 10^{-8} Torr; and the detector chamber has a base pressure of 10^{-10} Torr. During a pyrolysis run, the source, differential, and detector chambers have transient pressure increases that do not exceed 10^{-5}, 10^{-6}, and 10^{-7} Torr, respectively. The source and differential chambers are connected by a 4 mm diameter water-cooled copper aperture located in front of the sample holder. 57 mm beyond this aperture is a second aperture of 1 mm diameter leading to the detector chamber. This second aperture and the ionizer of the mass spectrometer are 12.7 mm apart. These two apertures define the detection axis, and a small window at the back of the mass

spectrometer and the adjustable mount of the mass spectrometer chamber allow for careful alignment of the ionizer and entire mass spectrometer along the detection axis. An adjustable sample mount is used to position the center of the sample on the detection axis.

The sample mount (**Figure 2.1b**) is placed in the source chamber such that the sample is located 9 mm away from the first aperture. This sample mount consists of two copper blocks, each acting as an electrode. Clamped across the copper electrodes are two pieces of FiberForm which encase the sample. The sample is heated by supplying current through the FiberForm. The back piece of FiberForm is 3 × 41 × 19 mm with a 6 mm diameter × 2 mm deep shallow cylindrical hole carved into its center for placement of the pure SC-1008 samples, 6.35 mm diameter × 2 mm deep hole for PICA-D, and 10 × 15 × 3 mm deep square hole for 3MDCP-IL. The top piece of FiberForm is the same height and length, but half as thick. With this FiberForm encasement ("sandwich"), the sample is heated from all sides. Current is supplied to the sample mount by a programable power supply (TKD-Lambda GEN 40-19) and controlled by a LabVIEW program which is coupled with the Extrel mass spectrometer software. The sample mount is cooled with a continuous flow of 20 °C water. Temperature is monitored by a 30 AWG type K bare wire thermocouple purchased from Omega, with wires welded at an angle of ~23° to produce a fine junction point. The individual thermocouple wires are inserted into a two-channel ceramic tube, and the thermocouple junction is pushed through the back piece of FiberForm and slightly into the cupped region that holds the sample. The thermocouple wires just behind the junction are adhered to the back of the FiberForm with a two-part ceramic adhesive (AREMCO Ceramabond 571-P), to ensure that the thermocouple

does not shift as the sample is heated. The sample is then placed into the FiberForm cup, and the FiberForm cover applies force on the sample to hold it against the thermocouple junction.

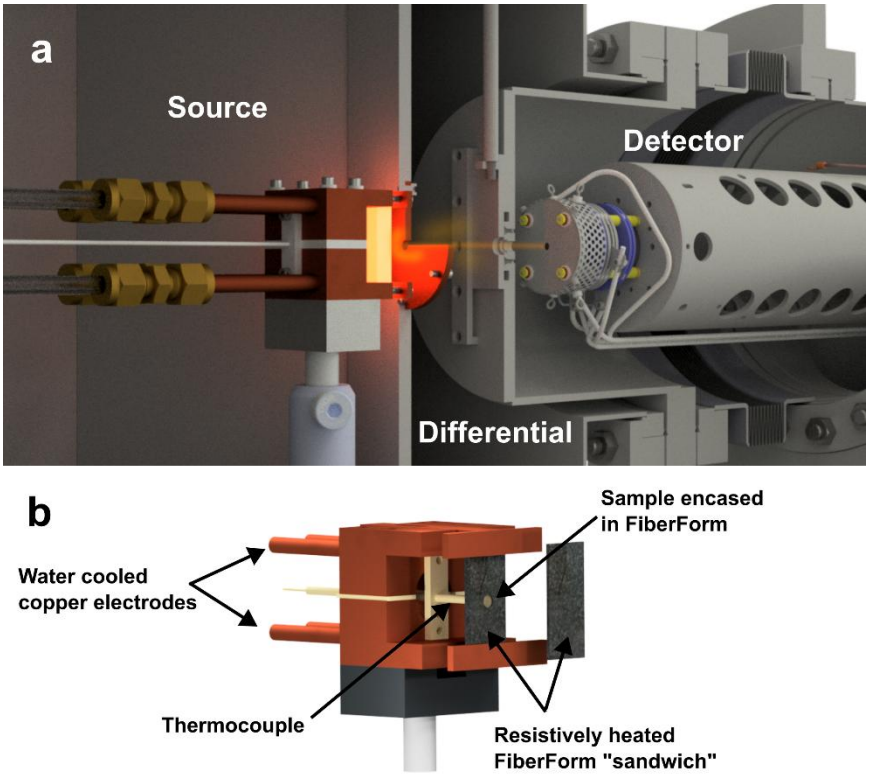

Figure 2.1 (a) Diagram of the experimental apparatus with source, differential, and detector chambers. The sample mount is placed in the source chamber. (b) The sample mount consists of water-cooled copper electrodes and a resistively heated FiberForm sample holder for heating the sample from all sides. A thermocouple is inserted through the back of the copper mount and held in direct contact with the sample.

2.2 Mass Spectrometer Library and Calibration

A library of mass spectra was generated to facilitate the derivation of molar yields from the raw data, and this library comprises 16 species, shown in **Table 2.1**, which either represent the major pyrolysis products or are indicators of certain reactions. N_2 was only used in the analysis of 3MDCP-IL. The 15 other species were chosen based on observations in the literature, proposed mechanisms, and previous results.[8] In the previous study by Bessire and Minton, 14 species were

chosen, with data collected over a range of mass-to-charge ratios, m/z = 1 - 150.[8] In the current study, the mass spectral range was extended to m/z = 0.5 - 200, allowing for an additional product, diphenyl ether, to be added to the library. Besides improving the accounting for the total mass of pyrolysis products, the detection of diphenyl ether is an indication of intermolecular condensation. All mass spectrometer library species were stable molecules, as it was assumed that, even if the initial decomposition mechanisms involve reactions to produce radical products, these radicals are likely to react to form stable products before exiting the material. Isomers of xylene, cresol, dimethyl phenol, and trimethyl phenol are not distinguished, as the mass spectra of the isomers of the respective products are almost identical. The isomers used to generate the library were o-xylene, o-cresol, 2,4-dimethyl phenol, and 2,4,6-trimethyl phenol, because these are more likely to form rather than isomers with meta substitution, as a result of the electron resonance of phenol which inhibits C-alkylation at the meta position during polymerization.[11]

Table 2.1 Assumed gaseous molecular products from the pyrolysis of phenolic resin.[c]

Permanent Gases	Condensable Gases
H_2	H_2O
CH_4	1-Propanol
CO	2-Propanol
CO_2	Benzene
N_2	Toluene
	Phenol
	Xylene
	Cresol
	Dimethyl Phenol
	Trimethyl Phenol
	Diphenyl Ether

[c]Specific isomers of o-xylene, o-cresol, 2,4-dimethy phenol, and 2,4,6-trimethyl phenol were used in the mass spectrometer library (see text).

The mass spectrometer reference library was generated by collecting mass spectra of individual molecular compounds with the same settings of the mass spectrometer that were used to collect mass spectra of pyrolysis gases. When collecting mass spectra of the permanent gases (H_2, CH_4, CO, CO_2, and N_2), each gas was introduced into the main chamber through an effusive nozzle with an orifice of 0.34 mm diameter placed 3 mm from the first aperture, with pressure controlled by a regulator and variable leak valve. Downstream of the valve, a capacitance manometer (Pfeiffer CM 363) was used to measure the pressure of the gas in the nozzle, which was on the order of 10^{-2} Torr. The other eleven species, which are condensable gases, were introduced into the main chamber through the same nozzle from a temperature-controlled stainless-steel vessel, with the pressure controlled by the variable leak valve and measured by the capacitance manometer, again on the order of 10^{-2} Torr. After collection and background subtraction, the mass spectrum for each compound was normalized such that the intensity of the highest peak was equal to 1.

Sensitivity correction factors for each product were obtained while creating the reference library. The relative flux of an individual compound, x, through the detector, I_x, is proportional to the measured number density in the detector times the average magnitude of the axial velocity of the compound exiting the nozzle, $\langle v_x \rangle$, corrected by a detector sensitivity correction factor, s_x.

$$I_x \propto N_{x,meas} \langle v_x \rangle s_x \tag{1}$$

To obtain the detector sensitivity correction factor for each compound, a known flux was directed into the mass spectrometer through the effusive nozzle. The flux was calculated using the relationship for flow through an effusive nozzle, as shown below, where A is the nozzle area, and P is the measured pressure upstream from the nozzle.

$$I_{x,effusive} \propto P_{x,effusive} \langle v_x \rangle A \tag{2}$$

The measured relative number density in the detector was then related to the known relative flux from the effusive nozzle.

$$P_{x,effusive}\langle v_x\rangle A \propto N_{x,meas,effusive}\langle v_x\rangle s_x \quad (3)$$

As the effusive flow has a Maxwell-Boltzmann distribution of speeds, the average velocity $\langle v_x\rangle$ has a $(T/m)^{1/2}$ dependence on the gas temperature, T, upstream of the nozzle and the molecular mass, m. The measurements with the effusive flows of pure gases (constant mass) were collected at constant temperature; therefore, the velocity terms in Eq. (3) cancel. In addition, the area, A, of the nozzle orifice was constant. Thus, the detector sensitivity factor is given by the following proportionality, which involves only two quantities that were measured.

$$s_x \propto \frac{P_{x,effusive}}{N_{x,meas,effusive}} \quad (4)$$

$P_{x,effusive}$ was measured with the capacitance manometer, and $N_{x,meas,effusive}$ was the value of the highest peak in the unnormalized, background-subtracted mass spectrum of each pure compound. The normalized mass spectra (where the highest peak is normalized to 1.0) and corresponding sensitivity correction factors for the 15 compounds in Table 1 comprise the mass spectrometer reference library.

2.3 Materials Preparation

Samples of Durite SC-1008[12] phenolic resole derived resin, were prepared and cut to size. First the commercial partially cured liquid resole resin underwent vacuum distillation to remove the isopropanol solvent. It was then cast into 6 × 15 mm rod molds and further cured in air according to the following curing program: 24 hrs. at 37.77 °C, 72 hrs. at 60 °C, 24 hrs. at 71.11 °C, 24 hrs. at 85 °C, 24 hrs. at 98.88 °C, 24 hrs. at 112.77 °C, 72 hrs. at 126.66 °C, and 24 hrs. at

137.77 °C. The rods were then cut into 2 × 6 mm discs using a diamond saw. Samples of PICA-D were prepared by cutting thin 2 mm thick pieces from a large block of PICA-D (supplied by NASA Ames) and then punching out circular disks of 6.35 mm in diameter with a thin metal cylinder. Samples of 3MDCP-IL (material supplied by NASA Ames) were prepared by first cutting a strip of material ~10 mm width, then pealing the weave, resulting in a strip 3 weave layers thick. Then, the ~10 mm width strip was further cut resulting in 10 × 15 mm × 3 weave thick rectangular samples. Many attempts were made to reduce the size of the samples for 3MDCP-IL; however, the material was very fragile and fell apart, limiting how small samples could be and affecting accuracy of mass measurements. The target weight of each sample of 3MDCP-IL was ~0.16 g. After making samples, all were stored in a vacuum desiccator until they were used for an experiment.

2.4 Experimental Procedures

Prior to collecting data for a pyrolyzing each sample, a thermocouple was attached to one strip of FiberForm, and both this back piece and the top piece of FiberForm were heated together without a sample in the center (see **Figure 2.1**). This FiberForm combination was repeatedly heated to 1200 °C in vacuum, allowing for outgassing and pyrolysis of any residual organic components in this commercial material. During this process, the parameters for the desired temperature gradients were optimized. After repeated temperature ramps of the FiberForm until volatile products were no longer detected and the heating program produced linear temperature gradients (with a minimum R^2 value of 0.999), the sample chamber was vented, the FiberForm was removed, and a sample was placed into the FiberForm holder.

For each temperature gradient, five pyrolysis runs were conducted. Each sample was first weighed on a semi microbalance (Ohaus Explorer) and then placed in the center of the FiberForm encasement and installed in the source chamber. The sample was then post-cured in the high vacuum source chamber at 150 °C for 24 hours to degas absorbed water. Once the post cure was complete and the sample had cooled to 25 °C, it was heated according to the programmed temperature ramp up to a final temperature of 1200 °C. During the heating, mass spectra were repeatedly collected from m/z = 0.5 to m/z = 200, with a resolution of m/z = 0.032 and a 0.5 s collection time for each full mass spectrum. An example of a raw data set of mass spectra for pure SC-1008 resin, which have been background-subtracted, can be seen in **Figure 2.2.** The temperature assigned to each mass spectrum is equal to the average sample temperature during the time the mass spectrum was acquired.

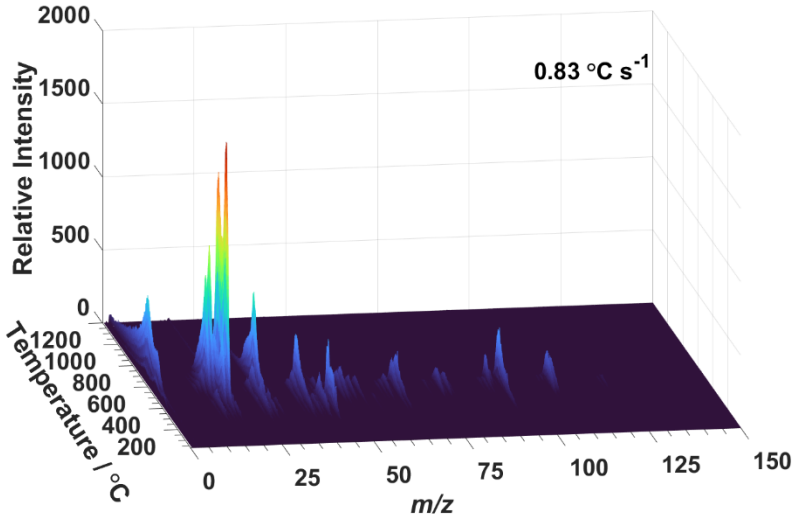

Figure 2.2 Complete set of mass spectra after background subtraction for one run of an SC-1008 sample at a temperature gradient of 0.83 °C s^{-1}. The mass range is truncated at m/z = 150, allowing for the signals from the dominant products at lower m/z ratios to be distinguished in this plot.

After each pyrolysis run, the charred sample was carefully removed and weighed so that the total mass loss of the sample could be determined. There was a slight mass loss during the post

curing of the sample at 150 °C, and this mass loss, which was determined by taking the average mass loss from several post-curing tests, was subtracted from the measured initial mass of the sample. The post cure mass loss for SC-1008 was 1.4 %, for PICA-D 2.13 %, and for 3MDCP-IL 1.12 %. Additionally, the average background mass spectrum was collected prior to each pyrolysis run and subtracted from each mass spectrum acquired during pyrolysis to isolate only the signal from pyrolysis. Overall average initial masses and total mass losses are reported in Appendix A **Table A.A.1** for pure SC-1008, Appendix B **Table A.B.1** for 3MDCP-IL, and Appendix C **Table A.C.1** for 3MDCP-IL.

2.5 Analysis of Mass Spectra

Relative molar yields were derived by fitting the background-subtracted mass spectra with the 15 individual mass spectra from the library (or 16 for 3MDCP-IL). A linear combination of these normalized single-compound mass spectra was optimized to the data by linear least squares fitting in MATLAB, where the coefficients were restricted to non-negative values. **Figure 2.3** shows a representative fit of a mass spectrum that was collected during pyrolysis of pure SC-1008 at a temperature gradient of 0.83 °C s^{-1}. The coefficients obtained by fitting each mass spectrum are proportional to the number densities of each product measured by the detector, $N_{x,meas}$. These number densities must be converted to flux to obtain relative molar yields. Under the assumption that pyrolysis gases evolve from the sample in thermal equilibrium at the sample temperature (i.e.,

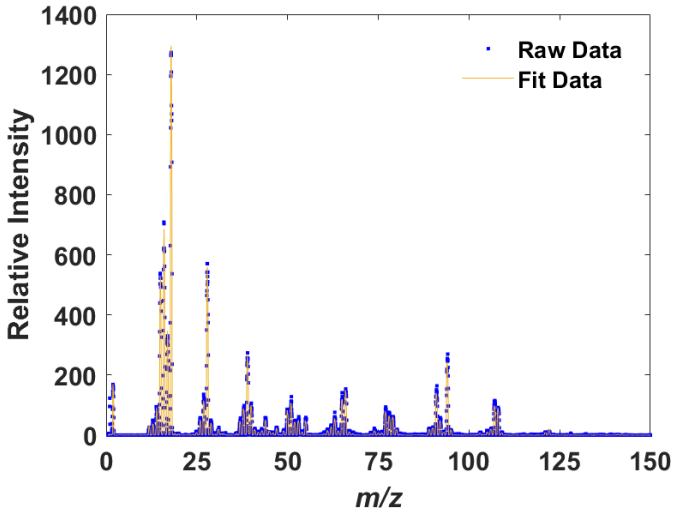

Figure 2.3 Representative fit of the mass spectrum of pyrolysis gases collected for pure SC-1008 at a sample temperature of 573 °C during a temperature ramp of 0.83 °C s^{-1}, using a linear combination of the library mass spectra of 15 pure compounds. The mass range is truncated at m/z = 150.

with a Maxwell-Boltzmann distribution of speeds), the relative flux, or molar yield, of each compound at each temperature during a pyrolysis run can be calculated using Eq. (1) and substituting for the average velocity $\langle v_x \rangle \propto \sqrt{\frac{T}{m_x}}$,[13] as shown below.

$$I_x(T) \propto N_{x,meas}(T) \sqrt{\frac{T}{m_x}} s_x$$

2.6 Analyzing Repeated Experiments

The relative molar yields as a function of temperature that were derived from five pyrolysis runs collected with a given temperature gradient had very similar shapes; however, the temperature-dependent molar yields for individual runs varied with respect to the temperature at which a given compound evolved from the sample. An example of this variability is shown in

Figure 2.4 a. It is possible to apply a temperature shift to each of the five temperature-dependent molar yield curves collected with a given temperature gradient and obtain a set of curves for each compound that have remarkably similar shapes (see example in **Figure 2.4 b**). The relative peak heights of the curves for the individual compounds that evolve during pyrolysis do appear to vary from run to run, which most likely results from variability in sample size, and will be accounted for later. The temperature shift, or apparent variability in the temperature range at which an individual compound evolves, was assumed to originate from measurement error of the sample temperature resulting from inconsistencies in the contact between the thermocouple junction and the sample. If the thermocouple does not make solid contact with the sample, then the actual sample temperature is higher than the temperature measured by the thermocouple. I assumed, then, that the pyrolysis run where the pyrolysis gases evolved at the highest temperatures provides a

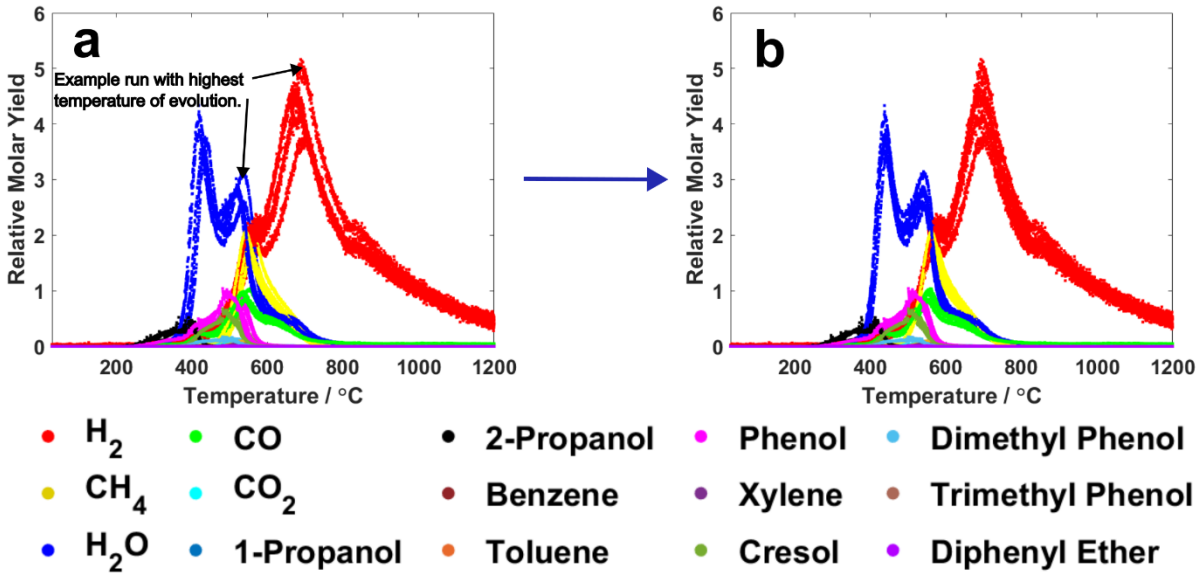

Figure 2.4 Relative molar yields for 15 species derived from five pyrolysis runs for pure SC-1008 with a temperature gradient of 0.83 °C s^{-1}, before (a) and after (b) shifting curves to coincide with molar yield curves derived from the temperature ramp where pyrolysis gases evolved at the highest apparent temperatures. The yields of H_2 and H_2O for the run where products evolved at the highest temperature are identified in (a).

lower limit to the temperatures at which these species evolved, and I shifted the relative molar yield curves derived from the four other pyrolysis runs at a given temperature ramp to coincide (as well as possible) with the corresponding relative molar yield curves derived from the pyrolysis run where the pyrolysis gases evolved with the highest measured temperatures. The temperature shift was calculated by taking the average difference of the peaks of H_2, H_2O, CH_4, and CO for each run compared to the corresponding peaks of the run with the highest-temperature evolution of pyrolysis products. After shifting, each set of relative molar yield curves, $I_x(T)$, was fit by a combination of Gaussian curves using Origin, with R^2 varying from 0.6 for a few species with very low relative molar yields to 0.99 for the more significant products. The fits of each set of five curves for each temperature gradient are reported for each material in their respective section as the relative molar yields as a function of temperature.

Another method of reporting the data is to plot mole fractions with respect to reaction extent. This representation of pyrolysis data is described by Gosma et. al. and collapses the data by removing temperature dependence.[5] As seen in **Figure 2.5**, plots of mole fraction as a function

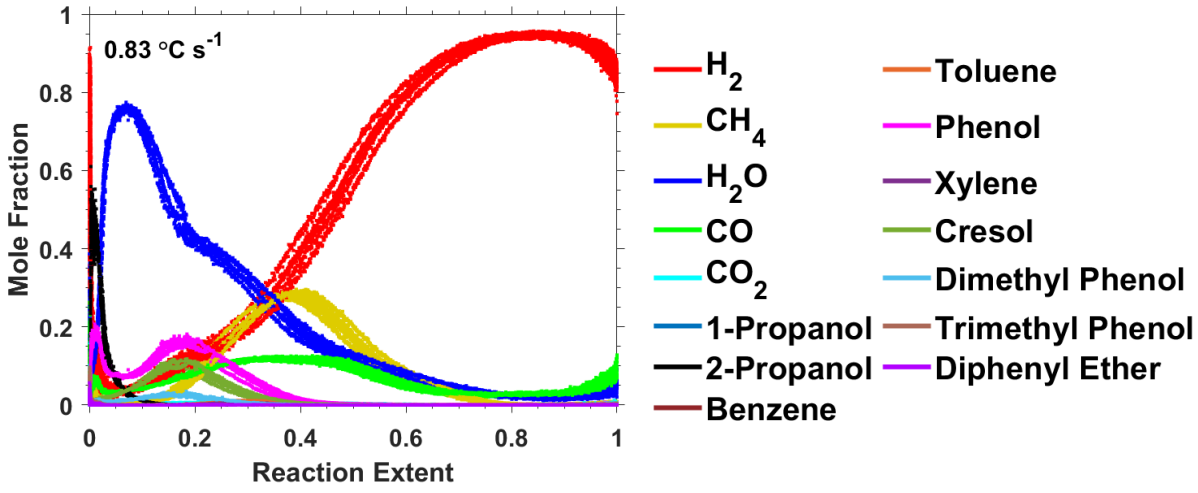

Figure 2.5 Plots of mole fraction vs. reaction extent for 15 species derived from five pyrolysis runs of pure SC-1008 resin with a temperature gradient of 0.83 °C s^{-1}.

reaction extent for five pyrolysis runs with an average temperature gradient of 0.83 °C s^{-1} overlap with each other well. Analogous plots of mole fractions with respect to reaction extent at the other temperature gradients are shown in Appendix A (**Figure A.A.1**), and they also exhibit good overlap. These results suggest that the temperature-dependent molar yield curves, such as those presented in **Figure 2.4**, do indeed vary only with overall linear shifts and not shifts between individual products.

2.7 Absolute Yields and Synthesized TGA Curves

The relative mass loss per compound at a given temperature, $m_x^r(T)$, can be obtained by multiplying the relative flux (relative molar yield) at that temperature, $I_x(T)$, by the respective molecular weight of each compound, MW_x.

$$m_x^r(T) = I_x(T) \cdot MW_x \tag{6}$$

The total relative mass loss, m^r, is then found by summing the relative mass loss, $m_x^r(T)$, over each compound, x, and temperature, T.

$$m^r = \sum_T \sum_x m_x^r(T) \tag{7}$$

Next, the mass loss fraction per compound at temperature T, $f_m^x(T)$, may be calculated for each pyrolysis run by dividing the relative mass loss per compound at temperature T by the total relative mass loss.

$$f_m^x(T) = \frac{m_x^r(T)}{m^r} \tag{8}$$

The average fractional mass loss as a function of temperature for a given temperature gradient can then be calculated by averaging each $f_m^x(T)$ for all five runs, and the mass loss from a given

compound as a function of temperature, $m_x(T)$, may be obtained by multiplying the average fractional mass loss, $f_{m,avg}^{x}(T)$, by the average total mass loss, TML_{avg}.

$$m_x(T) = f_{m,avg}^{x}(T) \cdot TML_{avg} \quad (9)$$

This mass loss assumes that the total mass loss comes from the evolution of the 15 or 16 gaseous pyrolysis compounds. To the extent that this assumption is correct, $m_x(T)$ may be considered to be the absolute mass yield of compound *x* that escapes from the sample in all directions at a given temperature for a given temperature gradient. Because the average total mass loss may be different for the experiments with different temperature gradients, I report normalized mass yields to aid comparison across all five temperature gradients. These normalized yields are determined by dividing $m_x(T)$ by the average total mass loss at the corresponding temperature gradient. The temperature-dependent, normalized mass yields of individual compounds for the five temperature gradients used are shown in.

Normalized molar yields were also derived. To determine absolute molar yields, $n_x(T)$, absolute mass yields for each compound were divided by their respective molecular weights. Normalized molar yields for each temperature gradient were then calculated by dividing by the calculated total molar yield (i.e., the sum of $n_x(T)$ for all compounds over the whole temperature range).

Standard deviations for the mass and molar yields were calculated for the five runs at each temperature gradient, and representative error bars are plotted in the relevant figures. Temperature deviations were calculated by comparing the five linear temperature rate fits, and monitoring their variation as time progressed. The variation between the actual temperature and fit, as well as the effect of the temperature shift when comparing the 5 runs, was not considered in the error bars, as the deviation from linearity was very small (R^2 = 0.99), and the approach of shifting the

temperature scale to align with that for the run with products evolving at the highest apparent temperatures was assumed to be valid.

Synthesized thermogravimetric analysis (TGA) curves were derived by summing the absolute mass yields over all compounds evolved at temperature T and converting to a percentage of mass remaining, as shown below, where M_o is the average initial sample mass.

$$\%m(T) = \frac{100}{M_o}[M_o - \sum_T m_x(T)] \quad (10)$$

2.8 Validation of Methodology

To test whether the molar yield calculations were accurate, a gas mixture with known mole fractions of CO_2 (0.5137), CH_4 (0.1009), CO (0.3575), and H_2 at (0.49023), was introduced into the source chamber through the effusive nozzle, with the set-up as described for the library mass spectra collection, with pressures of 4.6×10^{-2} and 3.4×10^{-2} Torr at room temperature. The measured percentages of each gas were calculated after background subtraction by fitting with the library of

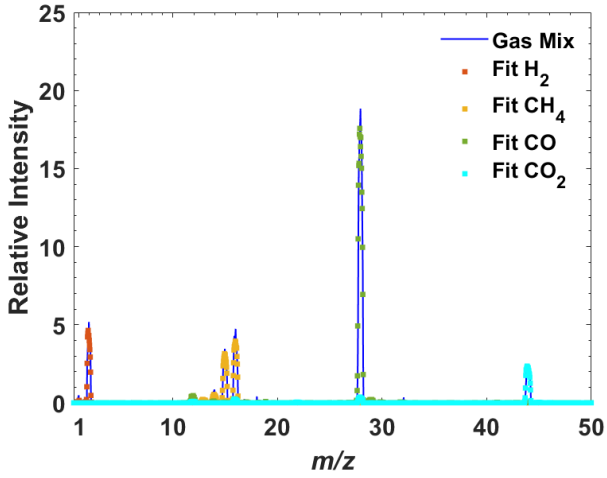

Figure 2.6 Fit to mass spectrum of mixed gas with known mole fractions of H_2, CH_4, CO, and CO_2, using the mass spectrometer library and the sensitivity factors that were derived for the analysis of pyrolysis data.

relevant compounds, applying corresponding detector sensitivity corrections, and finally deriving mole fractions (see **Figure 2.6**). Then these experimental results were compared to the known mole fractions of the gas mixture. The average percentage error across three trials was found to be 5.22 %, with the average mole fractions derived from the analysis procedure being 0.5141 for CO_2, 0.0947 for CH_4, 0.3409 for CO, and 0.5030 for H_2. Systematic errors are possible in the fitting; however, the errors appear random with chemical species in multiple test experiments. Therefore, it is likely that variation in the background and random errors from background subtraction contribute to the variability in percentage error.

To validate the processes of measuring temperature and calculating synthesized TGA curves, a synthesized TGA curve was compared to a standard TGA curve collected on a NETZSCH STA 449 F3 Jupiter simultaneous thermal analyzer at Sandia National Labs. The sample of SC-1008 resin used for the standard TGA was post cured under argon for 12 hrs. and stored in a desiccator; then the 18.863 mg sample was pulverized and allowed to outgas in the TGA apparatus for 15 minutes prior to the run. TGA curves with a temperature gradient of 0.83 °C s^{-1} were

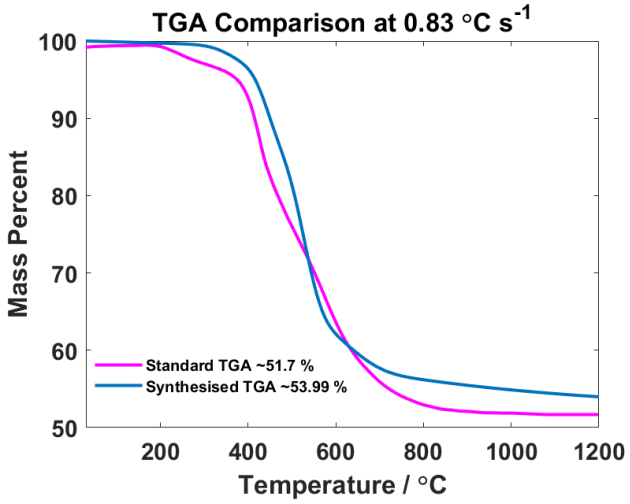

Figure 2.7 Standard TGA curve compared with synthesized TGA curve at a temperature gradient of 0.83 °C s^{-1}.

compared, as seen in **2.7**. The regions of steepest slope in the two TGA curves were very similar, indicating that the temperature measurements in our pyrolysis studies are likely accurate. There are, however, differences in the shape and total mass loss. The first difference is the slight mass gain in the traditional TGA curve between room temperature and 200 °C, which is an artifact from buoyancy effects.[14] Next, there is a dip from the outgassing of H_2O, isopropanol solvent, and residual phenol. This dip is more pronounced in the traditional TGA curve compared to that in the synthesized TGA curve, as a result of sample handling and post cure procedures (12 hrs. in argon vs. 24 hrs. in vacuum; pulverized vs. solid). As seen in **Figure 2.4**, the post cure procedures for the synthesized TGA of pure SC-1008 successfully removed all absorbed H_2O, which may not be the case for the traditional TGA. Despite the post cure procedures, the isopropanol solvent was not completely removed, also seen in **Figure 2.4**. The second dip in mass loss above 400 °C results from the initiation of decomposition reactions. After the dip from outgassing, the mass-loss curve appears to be slightly broader in the traditional TGA, likely as a result of the much larger sample size and subsequent increased thermal gradient.[14] Finally, additional absorbed H_2O would result in an increased total mass loss from the greater initial H_2O content of the pulverized sample. Pulverization could also lead to more efficient charring, resulting in greater mass loss.

Chapter 3

Pyrolysis of Pure SC-1008 Phenolic Resin

Most pyrolyzing ablative heat shields contain phenolic resin; therefore, an understanding of the thermal decomposition mechanisms of this material can provide a foundation upon which to develop improved materials response models, which can, in turn, lead to better heat shield design and performance prediction. With the goal of obtaining high-fidelity data on the thermal decomposition mechanisms of phenolic materials, a baseline study of the gaseous pyrolysis products from pure SC-1008 resole derived resin has been conducted. Product yields were detected by a mass spectrometer as a function of sample temperature, over the range of 25-1200 °C, at five linear temperature gradients with respect to time (0.83, 3.03, 5.83, 11.54, and 23.11 °C s^{-1}) using a method that is based on earlier work by Bessire and Minton.[8] Quantitative molar and mass yields of 15 gaseous products have been determined as a function of temperature, and thermogravimetric analysis curves have been synthesized from the temperature-dependent mass yield data and measurements of total mass loss. Both the molar and mass yields exhibit temperature-gradient dependencies, as decomposition mechanisms compete and the residence time at each temperature may be comparable to or faster than mass diffusion and heat conduction time scales. The total mass loss increases with an increase in the rate of change of temperature, as a result of the competition between condensation and scission reactions, which was proposed previously, and this competition combined with the direct breakdown of backbone phenolic groups contributes to the changing molar yields. The new high-fidelity pyrolysis data provide mechanistic insight into the thermal decompositions of pure SC-1008 phenolic resin that can be used as a benchmark for

understanding the chemistry and modeling of the pyrolysis of complex carbon phenolic composites such as PICA (phenolic impregnated carbon ablator).

3.1 Experiment and Results

Experimental setup, procedures, and data analysis were performed as described in **Chapter 2**, for the pyrolysis study of pure SC-1008 at five temperature gradients. The synthesized TGA curves (**Figure 3.1**), and molar (**Figure 3.2**) and mass yields (**Figure 3.3**) were used in conjunction with data and mechanisms from literature to identify the decomposition pathway, and how it changes with increasing temperature gradients.

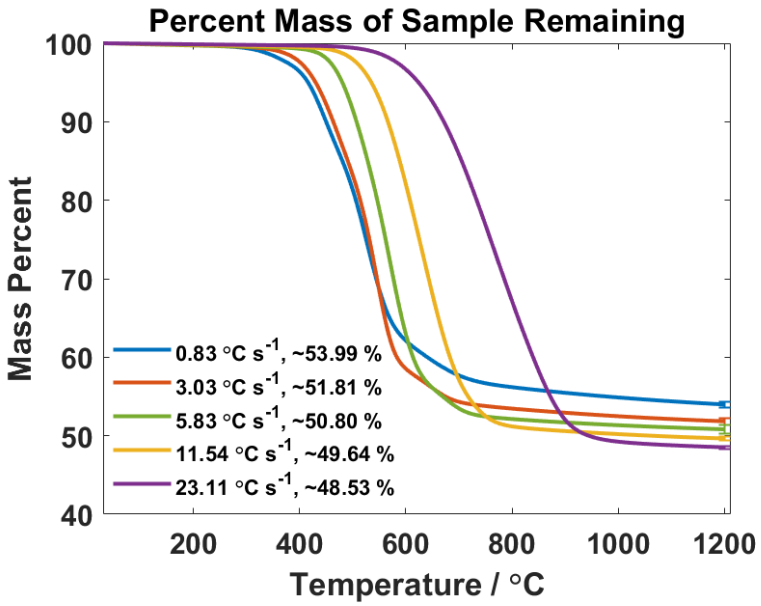

Figure 3.1 TGA curves synthesized from temperature-dependent mass yields for 15 compounds that evolved from pure SC-1008 resin during pyrolysis with five different temperature gradients, as shown in the legend. The percentages of mass loss at the end of each run (i.e., 1200 °C) are also shown in the legend.

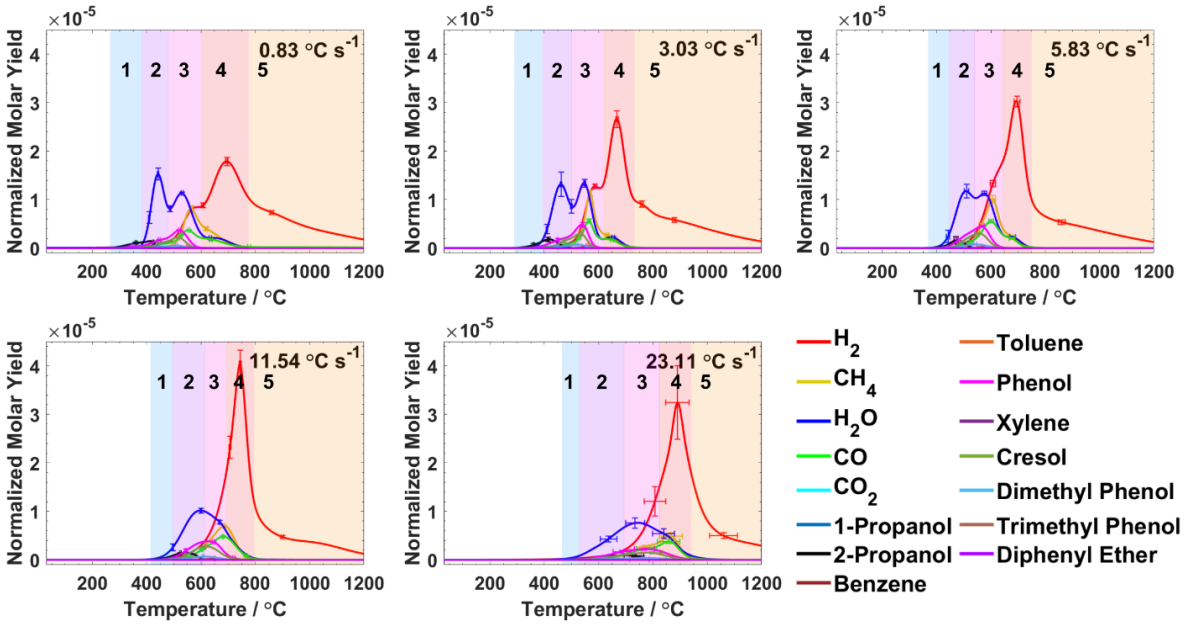

Figure 3.2 Temperature dependence of the molar yields of each gaseous pyrolysis compound normalized to the total molar yield of the 15 principal compounds that are assumed to evolve from pure SC-1008 during pyrolysis with five different temperature gradients, as indicated on each plot. Error bars represent ± 1σ for the five runs. Main regions of decomposition are identified by color and number. Expanded plots excluding H_2 and H_2O are shown in Appendix A **Figure A.A.3**.

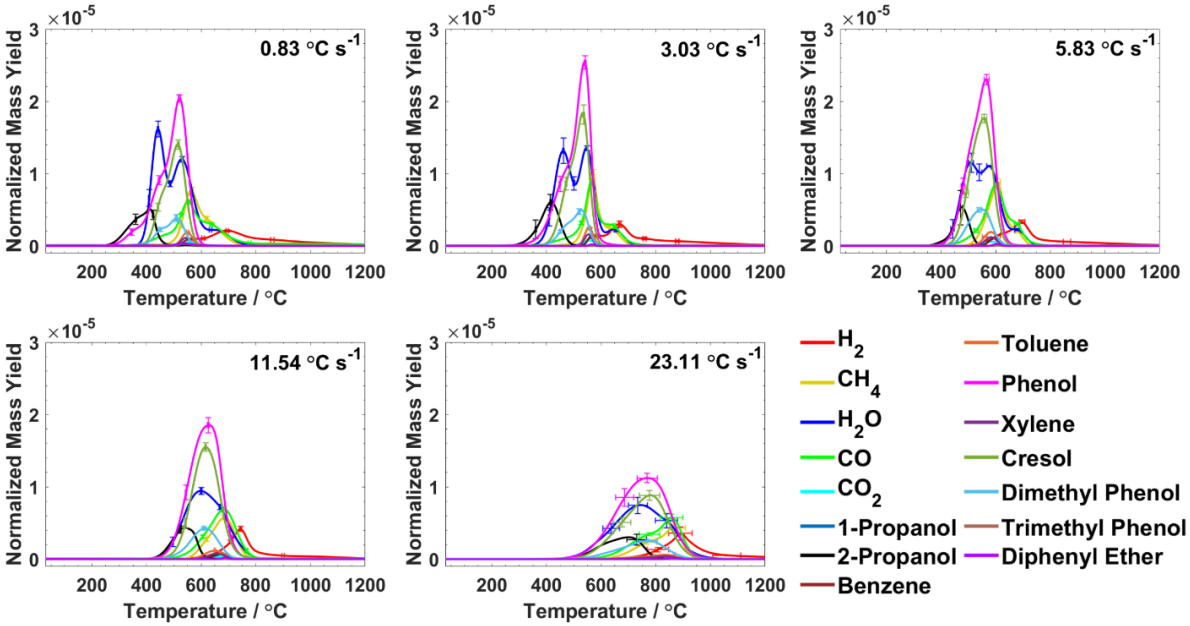

Figure 3.3 Temperature dependence of the mass yields normalized to the average total mass loss of 15 compounds that are assumed to evolve from pure SC-1008 during pyrolysis with five different temperature gradients (ramps), as indicated on each plot. Error bars represent ±1σ from the five runs.

3.2 Discussion of TGA Phenomena

As the temperature gradient is increased, four main changes are seen in the synthesized TGA curves (**Figure 3.1**): (1) shifting to higher temperatures, (2) smoothing, (3) mass loss over a broader temperature range, and (4) increasing total mass loss. The first three changes are caused by the reduced residence time at each temperature with increased temperature gradient, which may affect the reaction extent at each temperature, the diffusion rate, and the temperature uniformity. All reactions require an activation energy (or temperature) to initiate, as well as sufficient time at that temperature to release products. If the temperature changes rapidly on the time scale of a reaction, then products from that reaction will appear at a higher temperature than the temperature of initiation, resulting in a shift in the TGA curve toward higher temperatures.[15] As not all reactions require the same amount of time, their shifts may vary, leading to the overlapping of reactions and causing smoothing and broadening of the TGA curves. Shifting and broadening may also occur when the residence time at each temperature is shorter than the diffusion time of products out of the sample.[13,] This effect also causes an increase in internal pressure as products build up without time to diffuse, and this increased internal pressure is believed to suppress the volatilization of products, further shifting the release to higher temperatures.[15,17] It is clear that internal pressure build up occurs in the samples, as they were observed to crack significantly at high temperature gradients. Finally, because the sample is heated from all sides, a temperature difference between the center and surface occurs if the rate at which the measured surface temperature changes is faster than the rate of heat conduction through the sample. Thus, a high temperature gradient could broaden the mass-loss curves under conditions where the sample center and surfaces are at different stages of pyrolysis.[16] According to predictions by Nam and Seferis, a 2 cm thick carbon-phenolic composite pyrolyzed at 0.116 °C s^{-1} exhibited a maximum temperature difference

between the center and surface of around 50 °C.[16] The samples used in our study are about one tenth as thick; however, the temperature gradients are ≳10× higher; therefore, it is likely that a thermal gradient was present. Additionally, according to the International Confederation for Thermal Analysis and Calorimetry, during TGA experiments, a sample's mass multiplied by the temperature gradient should not exceed 0.1 mg °C min^{-1} to avoid thermal gradient and diffusion effects.[18] Given this guideline and the corresponding values of 3.176 - 81.514 mg °C min^{-1} in our experiments, such effects likely play a role in the observed data.

The final observed change with temperature gradient is the statistically significant increase in mass loss with increased temperature gradient. This observation is consistent with temperature-gradient-dependent TGA experiments in the literature, for example Stokes[19] observed an increase in mass loss from ~49 % to ~51 % weight between the temperature gradients of 5 and 16.7 °C s^{-1}, and is explained by preferential char forming (carbon preserving) pathways at lower temperature

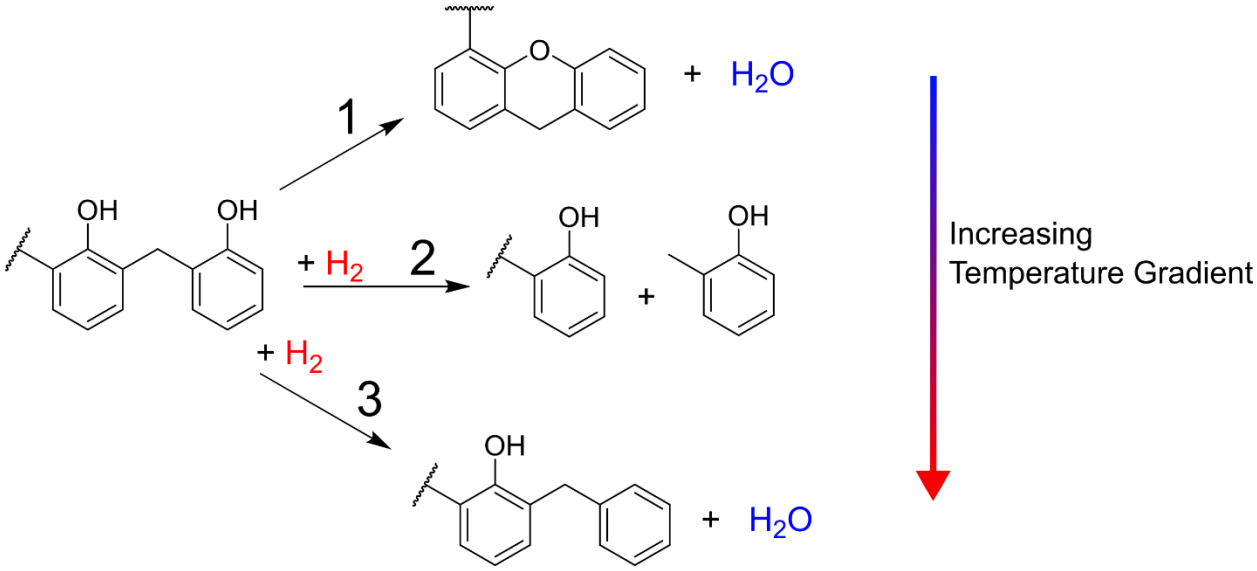

Figure 3.4 Three main competing reaction pathways during pyrolysis of SC-1008: (1) example of a water-producing condensation reaction at low temperature gradients, (2) example of methylene bridge scission at medium temperature gradients, and (3) example of the decomposition of phenol OH groups through dehydroxylation at the highest temperature gradients.

gradients.[15,20] For the pyrolysis of pure phenolic resin, the increased mass loss was attributed to the competition between three key reactions, shown in **Figure 3.4**, and how they overlap with increased temperature gradient. The first reactions to compete are condensation and scission reactions, as suggested by Bessire and Minton.[8] At low temperature gradients, there is sufficient residence time for many condensation reactions to occur (e.g., condensation reaction 1, **Figure 3.4)**, releasing H_2O and preserving carbon through the formation of thermally stable cross-linked ethers. As the temperature gradient increases, fewer condensation reactions have time to occur; therefore, the resin structure is less thermally stable, and there is an increase in the probability for methylene bridge scission reactions leading to carbon removal via volatile aromatics (e.g., reaction 2, **Figure 3.4**). Evidence for the competition between condensation and methylene bridge scission is seen by the decrease in H_2O formed from condensation reactions and the increase in scission products (i.e., phenol and its derivatives with increasing temperature gradients. The ratio of integrated molar yield of H_2O to the total molar yield of phenol and its derivatives is shown as a function of temperature gradient in **Figure 3.4**, where it may be seen that this ratio decreases with increasing temperature gradient from 0.83 to 11.54 °C s^{-1}. At the highest temperature gradient, 23.11 °C s^{-1}, the decomposition of backbone phenolic OH groups (e.g., dehydroxylation, reaction 3, **Figure 3.4**) becomes more competitive with methylene bridge scission reactions, leading to an increase in the molar ratio of H_2O compared to that of phenol and its derivatives, as seen in **Figure 3.5**. Phenolic OH groups remaining in the resin do not appear to decompose to CO until temperatures above 600 °C,[21] and as the temperature gradient increases, more phenol groups remain intact up to this temperature because the reduced residence time at each temperature suppresses the relatively slow initial condensation reactions, as well as methylene bridge scission.

As a result, H_2O yields from the breakdown of phenol OH groups increase across all temperature gradients.

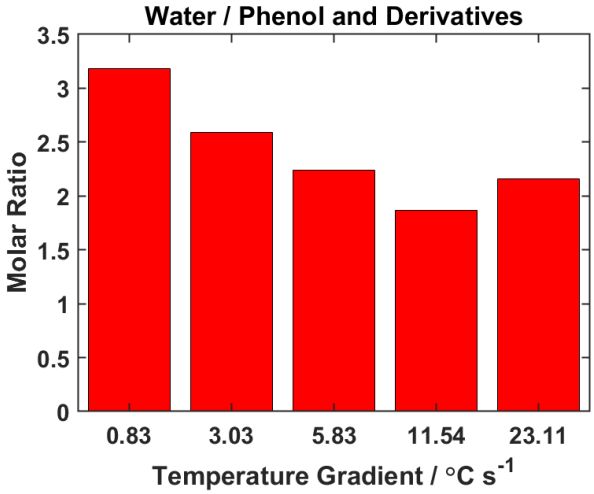

Figure 3.5 Ratio of integrated molar yield of H_2O to integrated molar yield of phenol and its derivatives for the temperature gradients of 0.83, 3.03, 5.83, 11.54, and 23.11 °C s^{-1}.

3.3 Temperature-Dependent Decomposition Mechanism

Five main thermal decomposition regions can be identified, and these regions are indicated in the plots of normalized molar yield as a function of temperature in **Figure 3.2**. The molar yield data collected at the lowest temperature gradient of 0.83 °C s^{-1} are used in this subsection to describe the decomposition mechanisms that distinguish the five regions. These regions are less distinguishable in reaction extent space, because at each point along reaction extent, the total molar yields sums to one, which can skew the importance of each reaction in the pyrolysis process.

In region 1, the main reactions release residual unreacted phenol as well as isopropanol, the latter of which is used as a solvent in the commercial SC-1008 resin.[12] There is a small molar ratio of ~0.03 for 1-propanol to 2-propanol; however, this could be the result of noise in the 2-propanol signal or trace contamination in the 2-propanol solvent. No H_2O is observed in this region

or at lower temperatures, suggesting that all absorbed H_2O was successfully removed during the 24-hr. post cure.

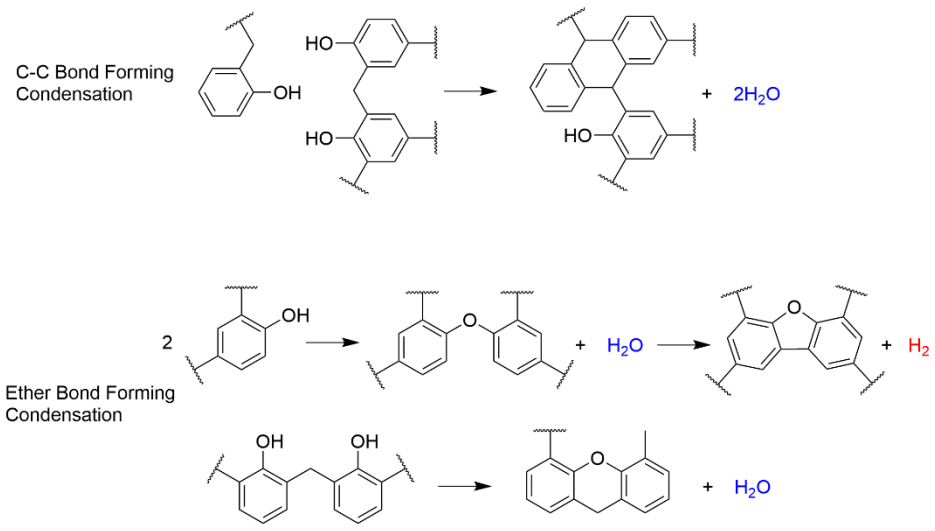

Figure 3.6 Examples of condensation reactions forming carbon-carbon cross links (top), ether bond forming intermolecular condensation to produce a diphenyl ether group that subsequently forms a dibenzofuran group (middle), and ether bond forming intramolecular condensation leading to a xanthene group (bottom).

The main products in region 2 come from thermal decomposition and are H_2O, H_2, phenols, and CO. Carbon-carbon bond forming condensation reactions lead to the production of H_2O, shown by the top mechanism in **Figure 3.6**.[8,22] Two possible types of condensation reactions release H_2O: carbon-carbon bond forming condensation and ether bond forming condensation.[8,23,24] Based on evidence from a pyrolysis experiment of phenolic resin labeled with deuterium performed by Yamashita and Ōuchi, the carbon-carbon bond forming condensation reaction occurs first.[25] This conclusion is also supported by the fact that the aliphatic hydrogens at a methylene bridge have the lowest bond dissociation energy of all the bonds in the virgin resin.[26,27] In region 2, residual methylol groups that formed during the original polymerization process of phenol and formaldehyde may dehydrogenate to form aldehydes (**Figure 3.7**). These aldehydes

can then directly decompose into CO or react with H_2O to form carboxylic acids, as shown in the

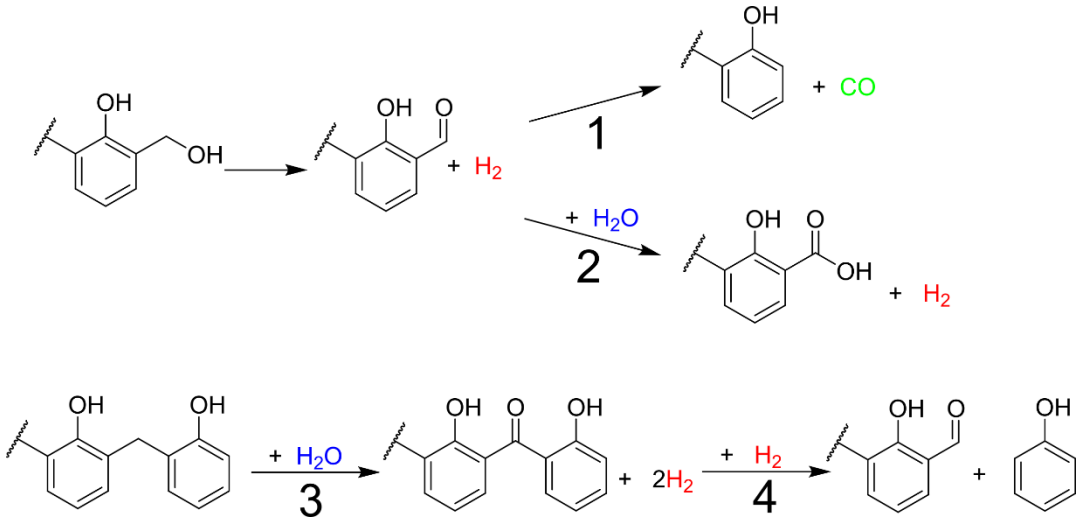

Figure 3.7 Dehydrogenation of methylol groups and (1) subsequent decomposition to CO or (2) oxidation by H_2O to form a carboxylic acid group. (3) Oxidation of a methylene bridge to form a ketone, such as a benzophenone group, shown here, and (4) subsequent decomposition to form an aldehyde group, which can further react through pathways 1 or 2.

second step in **Figure 3.7**.[8] A bridging ketone, such as a benzophenone group, could also be formed through the oxidation of a bridging methylene group, for example, by H_2O (reaction 3, **Figure 3.7)**, as proposed by Conley and Bieron.[28] Though benzophenone, with parent peak in its mass spectrum at *m/z* = 182, was not detected, these carbonyl absorption bands were observed as intermediate structures in IR experiments, with weak intensity.[23,28] Benzophenones were detected by Torres-Herrador et. al., and in the stepwise heating experiment, the sum of two benzophenone production pathways peaked at 400 °C which is within region 2.[29] It is unclear, however, whether or not the benzophenones were formed after trapping. Given that the degree of initial oxidation depends on surface area and that the samples were solid (low surface area), kept in a vacuum desiccator, and post cured in high vacuum, there should be minimal oxidation in the pristine resin.[28] Therefore, most of the oxidation should occur after H_2O is formed from condensation reactions and subsequently reacts with the resin. CO is formed after these oxidation reactions form an

aldehyde from methylol groups (reaction 1, **Figure 3.7**) and ketone intermediates that subsequently decompose to form an aldehyde (reactions 3 and 4, **Figure 3.7**).[30] The final reaction in region 2 is the scission of methylene bridges, which results mainly in phenol and cresol products (see **Figure 3.8**).[31] Cresol is formed at around half the molar yield of phenol. The scission of two methylene bridges also leads to dimethyl phenol formation at much less than the molar yield of cresol. Immediately after scission, these products are radicals, which are either stabilized by abstracting a hydrogen from the nearby resin structure or by reacting with H_2 in the gas phase.[11,31] Other experiments can provide more insight into the exact radical mechanisms involved in scission and hydrogen abstraction;[29] however, because the sample sizes in our experiments are relatively large and timescales are orders of magnitudes longer than those used in experiments which elucidate radical decomposition mechanisms, it is likely that most radical products are stabilized before exiting the resin. Additional evidence that radical products are stabilized is that the pyrolysis products and temperature dependent trends observed in this study are similar to those found in GC-

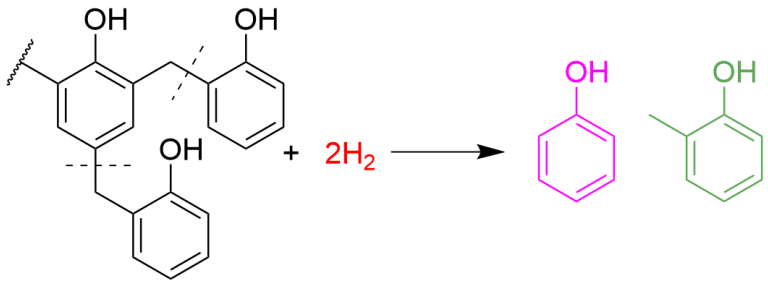

Figure 3.8 Example of a scission reaction involving a methylene bridge connecting a terminal phenol group, forming either phenol or cresol.

MS experiments, where the inherent nature of the experiment does not allow for the detection of radical products.[29,33]

Condensation reactions continue in region 3, and methylene bridge scission products reach their peak flux. The main products in region 3 are H_2O, H_2, CO, phenols, benzenes, CH_4, and CO_2. Ether bond forming condensation reactions (**Figure 3.6**) lead to H_2O.[8,22] Phenol, cresol, dimethyl phenol, and trimethyl phenol are released with the scission of the backbone methylene bridges,

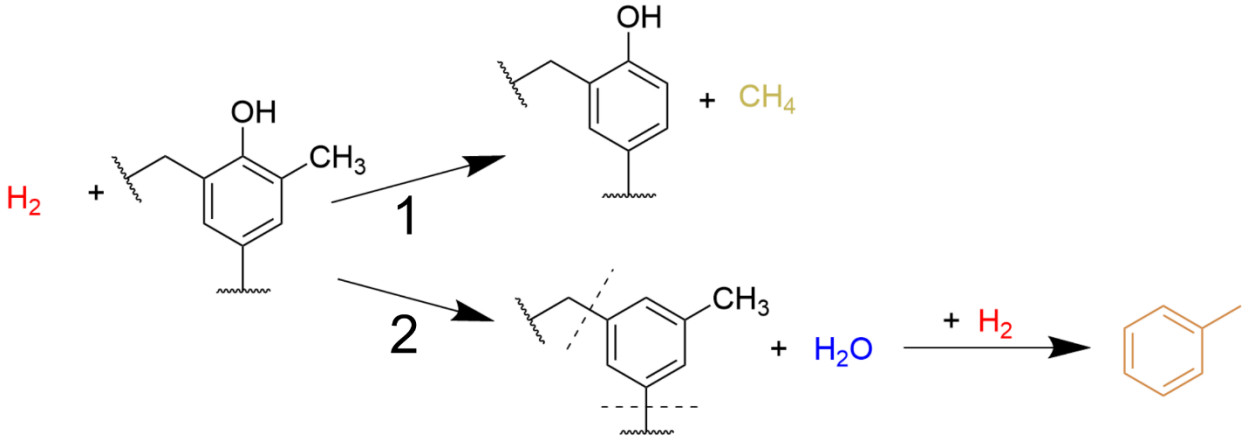

Figure 3.9. Reaction of a methylated phenol group attached to the main chain. (1) Demethylation and (2) dehydroxylation and subsequent scission.

similar to the mechanism of terminal phenol release (**Figure 3.8**).[8,31] After the scission of methylene bridges, CH_4 can be released with the dissociation of methylated phenol groups still attached to the main chain after the scission reactions, as seen by reaction 1 in **Figure 3.9**.[11,23,34] Dissociation of terminal methyl groups appears at higher temperatures than methylene bridge scission because the terminal methyl bond is more stable than the methylene bridge.[11] This reaction proceeds through a radical mechanism; however, as mentioned previously, it is likely that all radicals are stabilized before exiting the resin.[34] The dissociation of methyl groups from free phenol products may also result in CH_4; however, according to Buryan, for example, dimethyl phenol does not start to crack significantly until temperatures above 600 °C.[35] In our experiment

at a temperature gradient of 0.83 °C s^{-1}, aromatic compounds, including phenols, are not released beyond this 600 °C threshold (**Figure 3.2**); therefore, dissociation of methyl groups from free phenol products to produce CH_4 is unlikely. Dehydroxylation of the OH groups on phenols still attached to the main chain produces additional H_2O and leads to a pathway for the production of benzene, xylene, and toluene, as exemplified by reaction 2 in **Figure 3.9**.[11,35] Benzenes are a minor product, as the Ph–C bond is more likely to cleave (reaction 1, **Figure 3.9**) than the Ph–OH bond (reaction 2, **Figure 3.9**), because the OH group is an electron donor and lowers the bond dissociation energy of the Ph–C bond.[11] Carboxylic acid groups, which were formed in region 2 from secondary reactions with H_2O (**Figure 3.7**), decompose to produce a small yield of CO_2 (~10% of the total molar yield in region 3). Ether bridges formed early in region 3 through condensation reactions (**Figure 3.7**) decompose to form CO.[25,36] A mechanism for this source of CO has been proposed by Yamashita et. al. and is shown in **Figure 3.10**.[25] This mechanism may explain the high yields of CO, as the high H_2O yield indicates that ether bonds are formed in high yield in region 3.[25] The decomposition of these ether bonds was also observed by Day et. al. during the pyrolysis of poly(aryl-ether-ether-ketone).[37] Because ether bridges are more stable than methylene bridges, CO and benzene formation peaks at higher temperatures than the aromatic products from methylene bridge scission (see Appendix A **Figure A.A.3**). Finally, H_2 is produced as rings begin to fuse after the production of CH_4 and CO and the freeing of aromatic groups.[8,25]

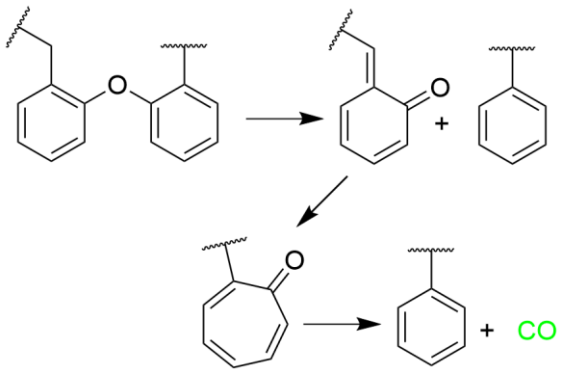

Figure 3.10 Formation of CO through the decomposition of an ether bridge.

Volatile aromatic hydrocarbons are no longer released in region 4, indicating that methylene bridge scission and crosslinking reactions have subsided, and the structure is characterized by large stable polycyclic aromatic hydrocarbons containing some remaining OH, methyl, and ether groups. The products in region 4 are H_2O and the permanent gases, H_2, CO, and CH_4. The polycyclic aromatic hydrocarbons grow and carbonize rapidly, signified by the peak in H_2 production. H_2O is formed in this region by dehydroxylation of OH groups on the polycyclic aromatic hydrocarbons, which is promoted by the production of H_2 and consequent increased pressure from carbonization, as observed by Cohen et. al. during the pyrolysis of phenolic resin in an H_2 atmosphere.[11] CH_4 continues to dissociate from methyl groups that originated as methylene bridges, with some CH_4 produced from the decomposition of aromatic rings, as observed in an experiment involving carbon-13 isotope marked phenolic resin.[25] At these high temperatures the phenolic OH bonds remaining in the polycyclic aromatic hydrocarbons may also decompose to CO after the O-H bond ruptures, as reported by Kundu et. al, with a proposed mechanism in **Figure 3.11**.[38] In this region, production of H_2O, CO, and CH_4 are all promoted by H_2 and as seen clearly at the temperature gradient dependent yields (**Figure 12**) there is a bump in yields of these products.

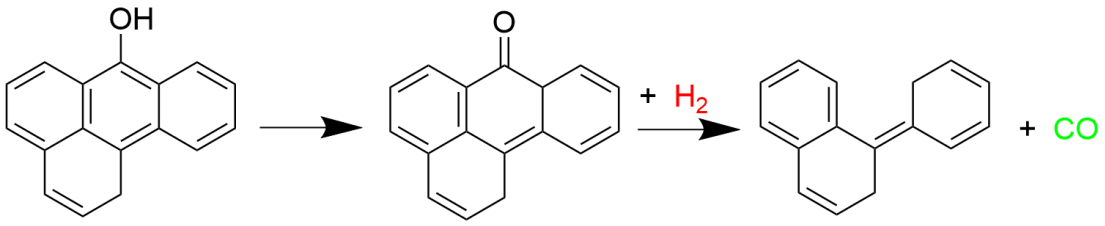

Figure 3.11 Decomposition of a phenolic OH group in a polycyclic aromatic hydrocarbon, leading to the formation of CO.

Most products in region 5 are the result of continued carbonization of the resin. The main product is H_2, which is released after the formation of carbon-carbon single, double, or possibly triple bonds within the polycyclic aromatic hydrocarbons, eventually leading to graphitic carbon. Although the H_2 production rate is decreasing at 1200 °C, it is still finite, indicating that the char has not been fully carbonized. The other significant product, albeit in small yield, is CO from the decomposition of more complex stable ethers, for example, xanthene or dibenzofuran, as shown in **Figure 3.12**, which are formed during condensation reactions in region 3.[8,38,39] The resulting aromatic ring structures after CO formation shown in **Figure 3.12** are speculated under the assumption that the most stable structures are formed.

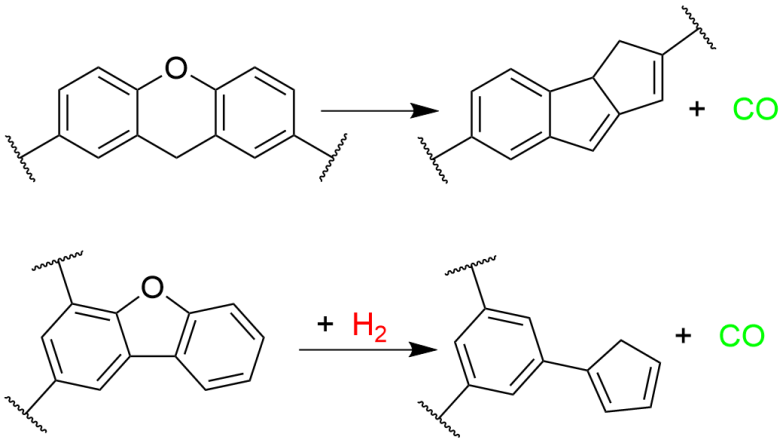

Figure 3.12 Formation of CO and subsequent fusing of rings through the decomposition of a xanthene or dibenzofuran functional group.

3.4 Temperature Gradient Dependencies

The plots of molar yield as a function of temperature in **Figure 3.2** indicate the 5 different regions of decomposition for the temperature gradients of 0.83, 3.03, 5.83, 11.54, and 23.11 °C s^{-1}. With increasing temperature gradient, these five regions shift and overlap as the residence time at each temperature decreases, as described in the context of the TGA curves in Section 4.1. These effects can also be seen in the reaction extent plots in Appendix A (**Figure A.A.1**), where the pyrolysis products, especially the heavier phenols, spread out across reaction extent.

As the temperature gradient increases, the release of unreacted phenol and isopropanol solvent in region 1 shifts to higher temperatures and overlaps with region 2, which may be caused by the diffusion rate of these gases out of the resin being less than or on the order of the rate of temperature increase. While all products tend to evolve at higher temperatures as the temperature gradient increases, the shift to higher-temperature evolution is less pronounced for H_2O than for isopropanol and phenol because H_2O is a smaller molecule and therefore has a higher diffusion rate.[40]

The slow carbon-carbon bond forming condensation reactions decrease with increasing temperature gradient in region 2, signified by the reduction in the first H_2O peak. With decreasing H_2O production from condensation reactions, secondary oxidation reactions forming carboxylic acids and ketones also decrease with increasing temperature gradient, as may be inferred by the decrease in CO_2 later in the decomposition process (i.e., at higher temperatures). The evolution of CO that is formed from the decomposition of aldehyde groups after the dehydrogenation of methylol groups (**Figure 3.7**) shifts to higher temperatures and evolves with CO from the decomposition of benzophenone groups as the temperature gradient increases. Methylene bridge scission to produce phenol, cresol, and dimethyl phenol from terminal phenols appears to increase

with the temperature gradient as these scission reactions outcompete the slower condensation reactions. These scission products also shift to higher temperatures with increasing temperature gradients, spanning a broader temperature range in their evolution and overlapping with phenols from outgassing or scission of *backbone* methylene bridges (which were proposed to occur after scission of terminal bridges by Parker and Winkler),[31] as diffusion rates and thermal gradients have an increasing effect on the yields.

Increasing temperature gradients have a strong effect on the molar yields of pyrolysis products in region 3, which is the region where the overall rate of mass loss is greatest. Scission of methylene bridges to produce phenols outcompetes condensation. However, as the temperature gradient increases, dehydroxylation of backbone phenolic OH groups becomes increasingly competitive with methylene bridge scission, because the relatively slow condensation reactions allow more phenol structures to remain intact up to high temperatures while the H_2 pressure concomitantly increases. The increase in phenolic structures in the presence of higher H_2 pressure results in a higher dehydroxylation probability and eventually causes a slight decrease in the evolution of phenols at the highest temperature gradient, along with an increase in H_2O (see **Figure 3.5**). H_2O from slow ether bond formation in region 3 decreases with an increase in temperature gradient and starts to overlap with H_2O produced by dehydroxylation in region 4. The molar yield of methyl substituted phenols increases with respect to unsubstituted phenol as the temperature gradient increases in region 3, with phenol still being dominant. In analogy with the phenols, the yields of methyl substituted benzenes (toluene and xylene) increase with respect to unsubstituted benzene as the temperature gradient increases, although the yields of the benzene compounds do not change dramatically with temperature gradient. This shift in the fraction of methylated phenols and benzenes with increasing temperature gradient might be the result of simultaneous scission

reactions of pendant and backbone methylene bridges, with a higher temperature gradient increasing the probability of scission at multiple bonding positions and therefore increasing the production of methyl substituted aromatics and decreasing the probability for dissociation of the more stable terminal Ph–CH_3 bonds.[11,29] The increasing H_2 production and consequent local pressure increase can promote radical reactions of hydrogen with OH and CH_x groups (**Figure 3.9**), as seen by Cohen et al.,[11] which could explain why there is no obvious decrease in CH_4 production with increasing temperature gradient even when there is an increase in methyl substituted vs. unsubstituted aromatics. With the decrease in slow condensation reactions in region 2 as the temperature gradient increases (**Figure 3.6**), there is less H_2O to react with carboxylic acid groups to produce CO_2; thus, the yield of CO_2 decreases at higher temperature gradients. In addition, with a reduction in condensation reactions, pathways for the formation of CO through the decomposition of ether bridges (e.g., **Figure 3.10**) become less likely, reducing the yield of CO in region 3 at higher temperature gradients. Finally, as the temperature gradient increases in region 3, the peak in the rate of carbonization resulting in H_2 production appears to increase and sharpen. And at temperature gradients above 5.83 °C s^{-1}, the production of H_2 through carbonization reactions blends with H_2 produced from these reactions in regions 4 and 5. The sharp peak in H_2 apparently reflects a buildup of H_2 pressure at high temperature gradients.

The yields of all products in region 4 (H_2, CO, CH_4, and H_2O) appear to increase with the temperature gradient. As mentioned above, as the temperature gradient increases, more phenol groups remain intact up to higher temperatures, indicating less crosslinking from condensation reactions at high temperatures; therefore, there is an increase in OH groups available for dehydroxylation to form H_2O (**Figure 3.9**) or decomposition to CO (**Figure 3.11**). After the phenol decomposes, ring fusing or cyclization leads to H_2 production. The resulting high concentration of

H_2 may also promote reactions with OH groups to form H_2O. H_2 internal pressure also increases with increasing temperature gradient from diffusion limitations, further increasing H_2O production and therefore its yield.

The relative molar yields of the products in region 5 remain very similar across all temperature gradients, where the continued carbonization of the charred resin is occurring. H_2 decreases with a similarly decreasing slope at all temperature gradients; however, as the temperature gradient increases, this trailing slope shifts to higher temperatures, indicating that there is insufficient time to carbonize the char completely. The main distinction of the pyrolysis in region 5 is at the lowest temperature gradient, where the decomposition of complex ethers, such as xanthene and dibenzofuran, produce CO, whose production decreases with increasing temperature gradient. This result indicates that condensation (**Figure 3.6**) reactions forming cyclic ether bonds are slow and decrease sharply with increasing temperature gradient above 0.83 °C s^{-1}. This decreasing CO production at high temperatures with increased temperature gradient was also observed by Bessire and Minton.[8]

3.5 Insights from New Experimental Methodology

While the previous experiment of Bessire and Minton[8] on the pyrolysis of PICA has been invaluable in the current experimental design and in the interpretation of the new data presented herein, the improvements made to the experimental methodology have increased the quantitative accuracy and precision of the data and have led to additional insights. The research grade mass spectrometer allows for high detection sensitivity, rapid scan rate, high mass resolution, and detection of a wide *m/z* range. The alignment of the sample along the detection axis, placement of the detector a short distance from the sample, and collimation of products with two apertures

produces a well-defined "beam" into the detector, with a well-defined velocity that allows relative product flux to be derived from number density measurements with the mass spectrometer. The utilization of a FiberForm heater and high product detection sensitivity makes it possible to use very small samples, minimizing thermal gradients and reducing temperature uncertainty. Small-gauge thermocouples that are held in the FiberForm with a ceramic adhesive provide additional improvement in temperature uncertainty. And standardized post-cure procedures in high vacuum reduce sample-to-sample variation. Although the material in this experiment is not PICA, as previously studied,[8] some new mechanistic insight for the decomposition of phenolic resin can still be gained. With the rapid scan rate, new details in the temperature-dependent product yields have been revealed, such as the identification of three peaks in the yield of water. The wide *m/z* detection range has enabled the detection of diphenyl ether, confirming its formation as a pyrolysis product. The ability to test small sample sizes and reduce thermal gradients and temperature lag resulted in narrower and more accurate yield vs. temperature distributions. The higher fidelity data led to synthesized TGA curves that shifted to higher temperatures with increased temperature gradient, matching well known trends in traditional TGA measurements[14,15,18] and giving confidence to the synthesized TGA curves. The observation of increased H_2O production between the two highest temperature gradients resulting from the increase in H_2 pressure and dehydroxylation of phenolic OH groups led to a proposed mechanism for the formation of benzene and derivatives (**Figure 3.9**). Thus, this new data set and mechanistic insight on the pyrolysis of pure SC-1008 resin provides a benchmark for future studies of phenolic resin containing composites. For example, the temperature gradient dependent quantitative molar yields of pure resin are essential for determining the influence of the carbon phase in carbon-phenolic composites. The pyrolysis of

PICA (specifically, PICA-Domestic) will be revisited with the new methodology, and further comparison with the previous study by Bessire and Minton will be made.

3.6 Conclusion

Mass and molar yields of 15 pyrolysis products have been quantified for pure SC-1008 phenolic resole derived resin as it decomposed at 5 temperature gradients, 0.83, 3.03, 5.83, 11.54, and 23.11 °C s^{-1}, across a temperature range of 25 to 1200 °C. TGA curves have been synthesized from the mass yields and total mass loss. Synthesized TGA curves and temperature measurements have been validated against a standard TGA measurement for the lowest temperature gradient of 0.83 °C s^{-1}. Both the molar yields and TGA curves show a clear dependence on temperature gradient, supporting work by Bessire and Minton[8] that the pyrolysis of phenolic resin materials is a non-equilibrium process. Thus, competition between reactions depends on the temperature gradient, causing the pyrolysis path to change. The decreasing residence time at each temperature resulting from higher temperature gradients also causes a shift in product yields to higher temperatures because of gas diffusion limitations. Thermal gradients between the surface and center of the sample cause the TGA curves to broaden, because the sample does not undergo uniform pyrolysis. The three main competing reactions were found to be (1) condensation reactions, which form ether or carbon-carbon cross links and H_2O, (2) methylene bridge scission reactions, which release mass through volatile aromatic hydrocarbons, and (3) breakdown of phenol groups (not previously observed), forming CO, or H_2O. Condensation reactions occur relatively slowly and form thermally stable, carbon-preserving ether bonds, and at higher temperature gradients, methylene bridge scission outcompetes condensation and results in enhanced mass loss through the production of phenol and its derivatives. The H_2O produced from

condensation reactions may proceed to oxidize the resin, leading to functional groups that decompose into CO and CO_2, though the observed yields indicate that this mechanism is not dominant. Methylene bridge scission reactions are faster, becoming more probable with increasing temperature gradient and release phenols. The decomposition of phenolic OH groups occurs at higher temperatures and is also relatively fast, with its rate increasing with temperature gradient. This process generally decreases the yield of large aromatic groups, which are products of methylene bridge scission. These three main competing reactions may follow radical mechanisms; however, it is likely that most, if not all, radical products are stabilized by hydrogen abstraction before exiting the resin. The competing decomposition pathways and product diffusion rates depend on the temperature gradient; therefore, the temperature gradient as a function of time will affect how a phenolic resin behaves in a thermal protection system. For example, thermal transport, chemical reactions, and boundary layer radiation are affected by pyrolysis gases blown out of the material. With this high-fidelity data on the pyrolysis pure phenolic SC-1008 resin, greater insight into the thermal decomposition mechanisms has been obtained and can now be applied to understanding the mechanisms of carbon-phenolic composites and material response modeling.

Chapter 4

Pyrolysis of PICA-D

The amount of thermal transport between an entry vehicle thermal protection system (TPS) and the boundary layer depends on the quantity of gaseous products produced during the pyrolysis of the heat shield material. Part of the function of a thermal response model is to predict this thermal transport, however, currently discrepancies between state-of-the-art models and flight data undermine the reliability of such models. For models to accurately capture heat transport, data on pyrolysis products from heat shield materials is needed. For this purpose, high fidelity data has been obtained on the pyrolysis products of PICA-D (phenolic impregnated carbon ablator – domestic), a carbon-phenolic composite, as a function of sample temperature, over a ranges of 25-1200 °C, at five linear temperature gradients with respect to time (1.08, 3.15, 5.92, 12.55, and 24.67 °C s^{-1}) using the method that was previously used to study the pyrolysis of pure SC-1008 phenolic resin. Absolute and normalized molar and mass yields of 15 gaseous products have been determined as a function of temperature, and thermogravimetric analysis (TGA) curves have been synthesized from the absolute mass yields. The yields and TGA curves exhibit slight temperature gradient dependencies, however, these dependencies are not nearly as significant as seen with pure SC-1008 resin because of the decreased density. Comparison of the yields of PICA-D and pure resin led to the identification of interactions via additional condensation reactions occurring in PICA-D between the resin and oxidized species on the carbon fibers. This new high-fidelity data has proven that the density of the material and whether carbon effects the pyrolysis mechanisms of phenolic resin.

4.1 Experiment and Results

Experimental setup, procedures, and data analysis were performed as described in **Chapter 2**, for the pyrolysis study of PICA-D at five temperature gradients. The synthesized TGA curves (**Figure 4.1**), and molar (**Figure 4.2**) and mass yields (**Figure 4.3**) were used in conjunction with data and mechanisms from literature to identify the decomposition pathway, and how it changes with increasing temperature gradients, and the contributions of the carbon fibers.

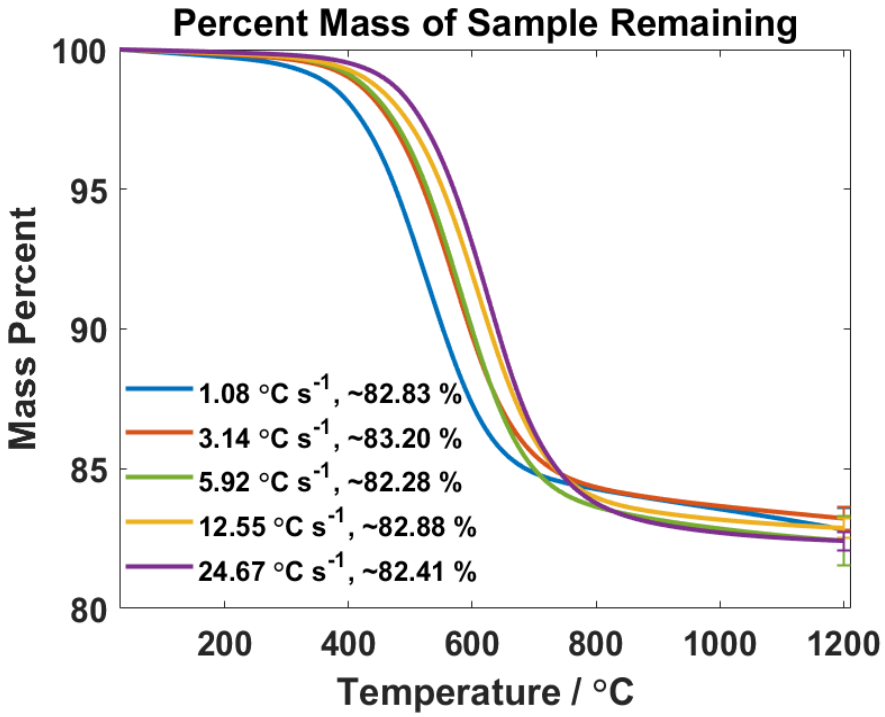

Figure 4.1 TGA curves synthesized from temperature-dependent mass for 15 compounds that evolved from PICA-D during pyrolysis with five different temperature gradients, as shown in the legend. The percentages of mass loss at the end of each run (i.e., 1200 °C) are also shown in the legend.

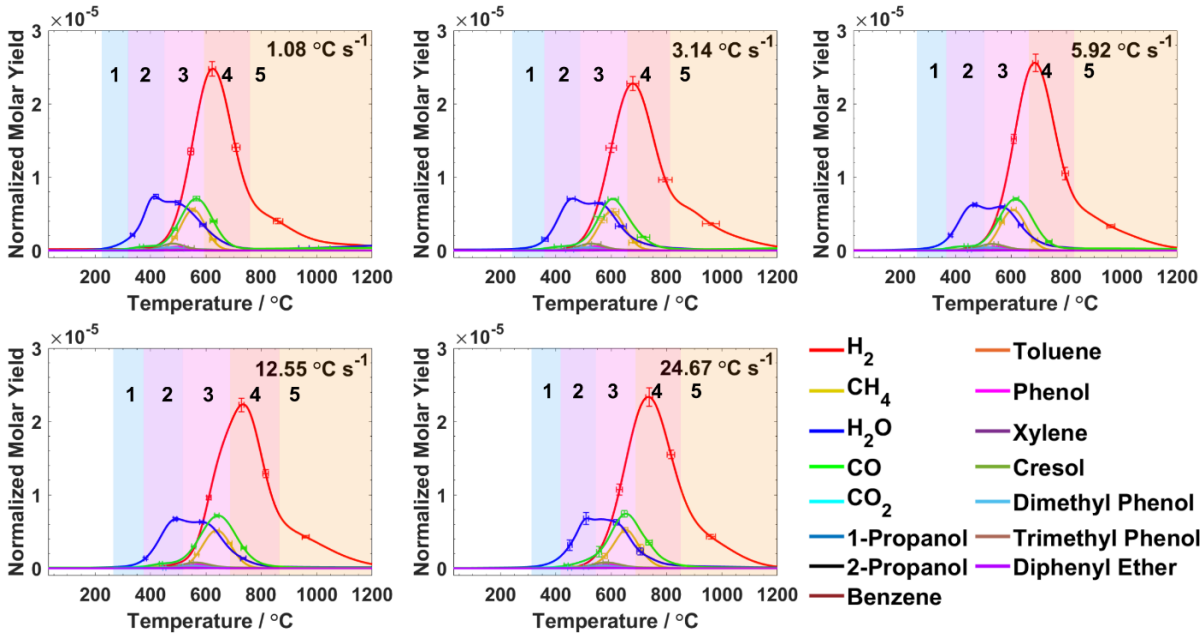

Figure 4.2 Temperature dependence of the molar yields of each gaseous pyrolysis compound normalized to the total molar yield of the 15 principal compounds that are assumed to evolve from PICA-D during pyrolysis with five different temperature gradients, as indicated on each plot. Error bars represent ± 1σ for the five runs. Expanded plots excluding some high yield products are shown in Appendix B **Figures A.B.1 and A.B.2.**

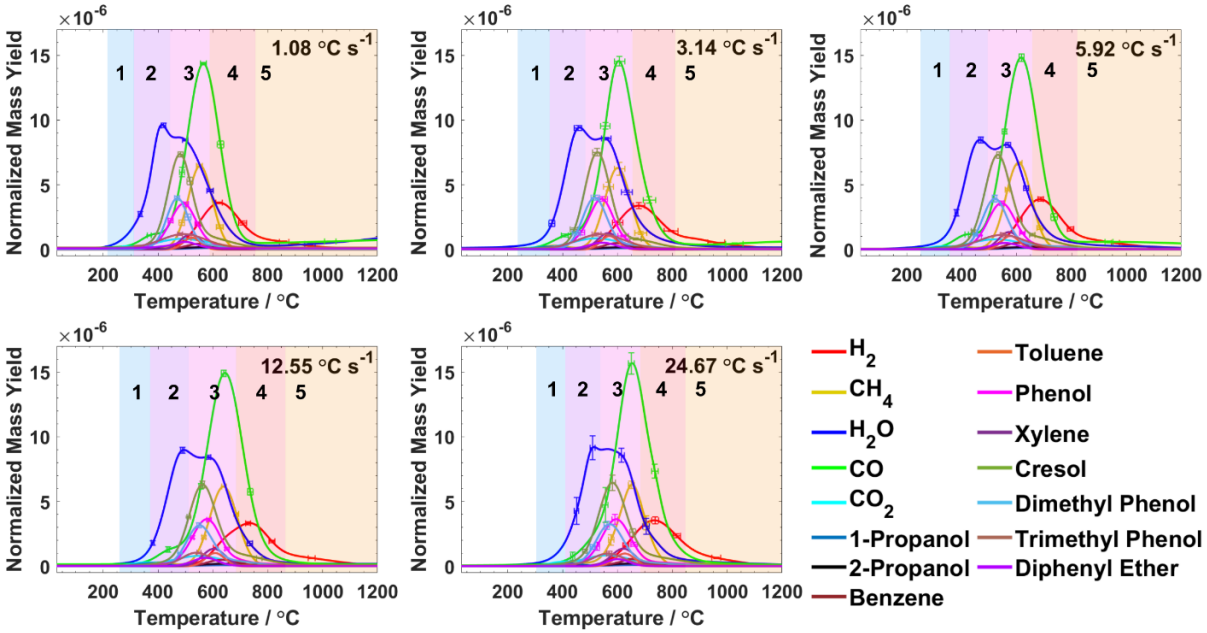

Figure 4.3 Temperature dependence of the mass yields normalized to the average total mass loss of 15 compounds that are assumed to evolve from PICA-D during pyrolysis with five different temperature gradients, as indicated on each plot. Error bars represent ±1σ from the five runs. Main regions of decomposition are identified by color and number.

4.2 Discussion of TGA Phenomena

As temperature gradient is increased, synthesized TGA curves (**Figure 4.1**) shift to higher temperatures, mass loss broadens over a wider range of temperatures, and change in slope above 900 °C. The shifting to right and slight broadening with increasing temperature gradient is a well-known trend seen in TGA data, caused by the shortening residence time at each temperature with increased temperature gradient.[14,15,18] The shortening residence time may affect the reaction extent at each temperature and the diffusion rate, which both lead to a delay or increase in the temperature at which a specific product is observed, shifting the yields to higher temperatures. The shortening of residence time may also affect temperature uniformity, as temperature gradients become on the order of or faster than heat conduction rates. Unlike pure phenolic resin, PICA-D is porous and conductive, therefore both particle and thermal diffusion rates likely do not play as important of a role in shifting to higher temperatures. That is why pure resin TGA curves have much more pronounced shifting and broadening.

The decrease in the slope of mass loss at temperatures above 900 °C is from the decrease in CO production at high temperatures with increasing temperature gradient. This is from the decrease in stable ether bond forming condensation reactions, such as the formation of benzofuran and xanthene (**Figure 3.6**). As the temperature changes begins to occur more rapidly, there is less time for condensation reactions which produce the stable cyclic ether bonds.[38,39]

Unlike pure resin, there is no statistically significant increase in mass loss with increased temperature gradient. This result could be from three factors: (1) nonuniformity between samples, (2) increased probability for crosslinking reactions, and (3) less competition between condensation and methylene bridge scission reactions. The process of making PICA-D is not publicly known

but does involve impregnating a large block of FiberForm with phenolic resin, and then subsequent curing. Because the blocks of FiberForm are large, the phenolic resin may not seep uniformly throughout the entire block, leading to nonuniformities in phenolic resin density. This could introduce variability in mass loss, inhibiting the detection of a temperature gradient dependence in the overall mass loss. The second factor is the increase in condensation reactions in PICA-D compared to pure phenolic resin pyrolysis. The increase in condensation in PICA-D is from additional reactions between oxidized species on the carbon fibers and resin, such as carboxylic acid groups, ketone groups, or OH groups, which leads to increased preservation of carbon through the formation of stable bonds, reducing the likelihood of methylene bridge scission.[41] These condensation reactions with the carbon fibers may occur during the original curing of the resin, post curing, or during pyrolysis. Additional evidence for an increased amount of condensation reactions can be found when mathematically recreating the density of PICA-D as a combination of the pure resin and FiberForm in an arbitrary volume. The estimated total mass loss of this recreated PICA-D is greater than that of true PICA-D, meaning the charr yield of resin in true PICA-D is greater than that of the pure resin. A similar phenomenon was observed by Yang et. al., when comparing the weighted average value of mass loss of a combination of coal tar pitch (which contains lots of polyaromatic hydrocarbons) and phenolic resin to the actual mass loss of a mixture of coal tar pitch and phenolic resin and found that the final mass loss of the mixture was lower than the mathematical weighted average, of which they claim is a result of interaction between the PAHs and phenolic resin.[42] The third reason that there is no overall mass loss trend is from less distinguishment and competition between condensation and methylene bridge scission reactions with increasing temperature gradient, as opposed to pure phenolic resin, because there is this overall increase in condensation reactions and less methylene bridge scission. Because PICA-D is

porous, there is less buildup of internal H_2 pressure to promote methylene bridge scission as the temperature gradient is increased. Instead, it appears that all aromatic products decrease slightly with an increasing temperature gradient compared to H_2 (see **Figure 4.4**). This trend is also seen in the ratio of H_2 to phenol and derivatives.

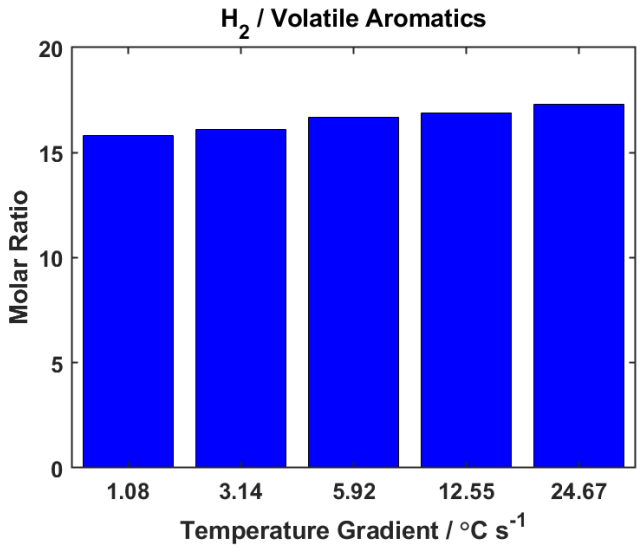

Figure 4.4 Ratio of integrated molar yield of H_2 to integrated molar yield of all volatile aromatic compounds for the temperature gradients of 1.08, 3.14, 5.92, 12.55, and 24.67 °C s^{-1}.

4.3 Temperature-Dependent Decomposition Mechanism

The temperature dependent decomposition of PICA-D can be broken down into 5 main regions (**Figures 4.2** and **4.3**) similar to the decomposition of pure SC-1008. Though the general mechanisms and reactions are the same, the temperature dependent yields in each region for PICA-D, however, are quite different from those of the pure resin as a result of the lower density, curing procedures, and presence of carbon fibers. In region 1, there is no outgassing of trapped residual

phenol like there is in pure resin, resulting from the different preparation and curing procedures, which could involve higher temperatures than the procedures used for pure resin. Instead, the main product in region 1 for PICA-D is the release of H_2O, which could be formed through two different mechanisms. First, H_2O can chemisorb to carboxylic acid groups present in the resin or on the FiberForm. Zeng et al. predicts that the strength of H_2O affinity for carboxyl functional groups decreases with increasing temperature, and drops off significantly at temperature of around 180 °C, above the 150 °C post cure temperature, meaning it is likely that not all chemisorbed H_2O was removed during the post cure.[43] The second possible source of H_2O is from the reaction of two adjacent carboxylic acid groups to form a carboxylic anhydride, for which Rosillo-Lopez et al. reported to occur around 285 °C.[44] Carboxylic acid groups appear to be present in the FiberForm of PICA-D, as shown by **Figure 4.5,** where in the pyrolysis of FiberForm CO_2 is produced. Both the above sources of H_2O could occur within the resin or FiberForm, since H_2O was also seen

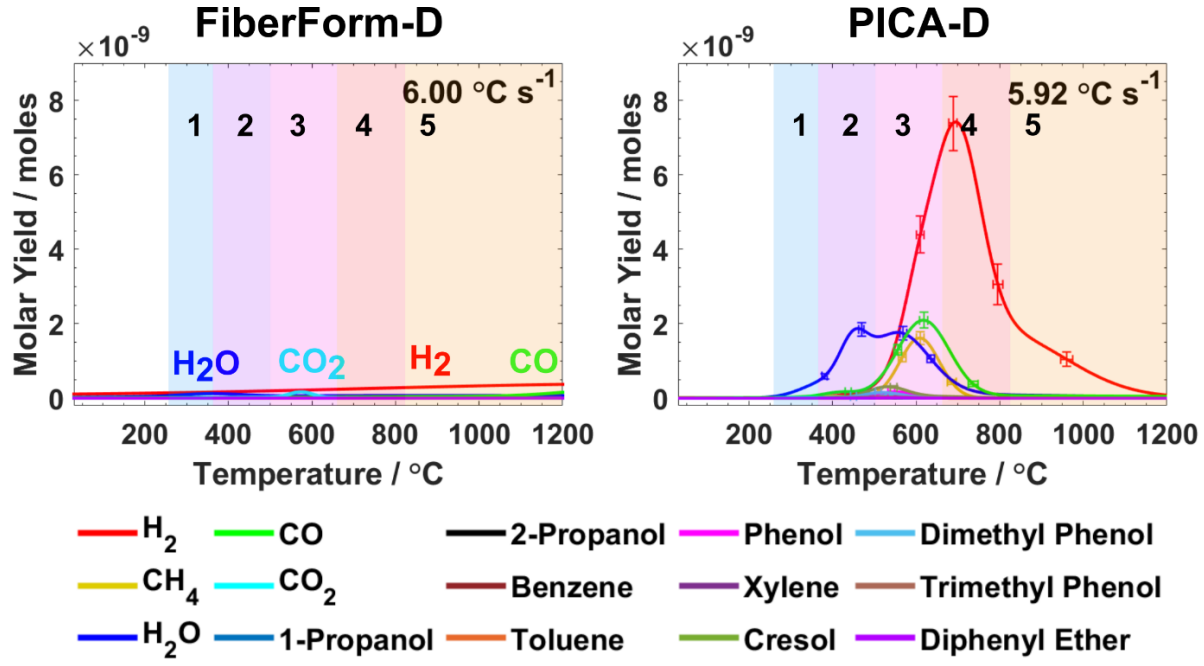

Figure 4.5 Comparison from the pyrolysis of lyocell derived FiberForm and PICA-D at the temperature gradient of ~ 6 °C s^{-1}, with the five regions of decomposition highlighted.

inthis region in the pyrolysis of FiberForm alone (**Figure 4.5)**; however, it is likely that the majority of the anhydrides are formed in the FiberForm, because the reaction requires two adjacent carboxylic acid groups as seen in **Figure 4.6**.[44] The minor products in region 1 are a small amount of propanol, likely leftover solvent, and a small amount of CO_2 from the decomposition of carboxylic acid groups that were initially present and that did not react to form a carboxylic anhydride (see Appendix A **Figure A.B.2**).

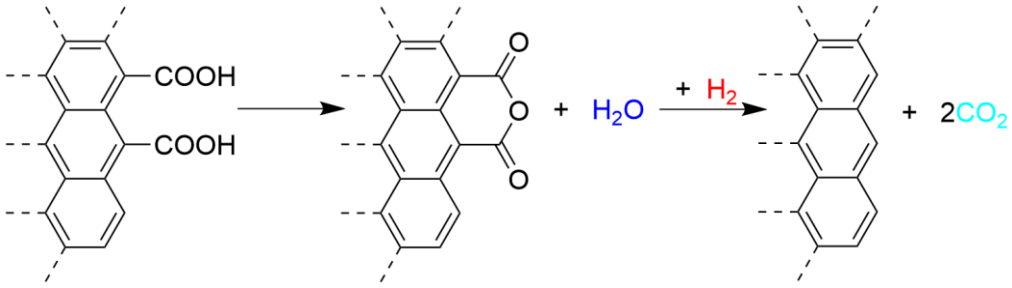

Figure 4.6 Reaction of two carboxylic acid groups to form a carboxylic anhydride and H_2O, and subsequent decomposition to CO_2 at higher temperatures.

The main products in region 2 are H_2O, CO, and CH_4. Some methylene bridge scission also begins to occur towards the end of region 2 as seen by the release of small amounts of phenol, cresol, dimethyl phenol, and trimethyl phenol (**Figure 3.8**); however, there is no distinct peak from the scission of terminal phenol groups as seen in pure resin. This is possibly a result of the increase in crosslinking and condensation that has already occurred between the resin and carbon fiber phases, or in the resin from different curing procedures. H_2O in region 2 is formed from carbon-carbon bond forming condensation reactions (**Figure 3.6**) within the resin structure and between the resin and FiberForm. CO in this region is formed after the dehydrogenation of methylol groups remaining in the resin and subsequent decomposition to CO, or from ketone groups such as benzophenone, formed after oxidation by H_2O of methylene bridges (**Figure 3.7**).[28] H_2O may also react after dehydrogenation of a methylol group to form a carboxylic acid group. PICA-D has a

much greater surface area and unknown handling history, which could mean it has a higher degree of initial oxidation compared to pure resin, explaining why CO in region two has a relatively higher yield for PICA-D than for pure resin. There is a clear distinct peak in CH_4 production before the appearance of scission products, something not seen in products from pure resin pyrolysis (see Appendix B **Figure A.B.1**). The production of CH_4 could possibly be from a reaction between H_2O and FiberForm, catalyzed by residual base that was used during the polymerization, or sodium contamination in FiberForm. Cabrera et al. have shown that graphene dipped in an NaOH solution then air dried reacts with H_2O to form CH_4 and CO at temperatures between 227 - 377 °C.[45] Even if there were some residual basic catalyst in the pure phenolic resin, this reaction would not be seen because there is no graphitic carbon at these temperatures.

In region 3, ether bond forming condensation reactions between the resin or between the resin and oxidized species in the FiberForm release high yields of H_2O (**Figure 3.6**).[41] Some H_2O may also formed towards the end of region 3 through dehydroxylation of phenolic OH groups (**Figure 3.9**). Ether bonds that are not cyclic subsequently decompose to form CO (**Figure 3.10**), whereas cyclic ether bonds such as dibenzofuran or xanthese groups remain in the structure. Ether bonds between the resin and oxidized species in FiberForm that may have also formed during curing,[41] will also decompose in region 3, contributing to the slightly greater peak in the yield of CO compared to H_2O (**Figure 4.2**). In the pure resin, the yield of CO is not greater than the yield of H_2O, because there is no oxidized carbon fibers to facilitate an increase in ether bond forming condensation during the curing or pyrolysis processes. Carboxylic anhydrides and oxidized species from secondary H_2O reactions, whether within the resin or the FiberForm phases, release CO_2 over the temperature range of 400 – 600 °C, the same temperature range as seen by Chen et al. during the annealing of oxidized graphene sheets.[46] Because FiberForm contributes to the CO_2

production, (**Figure 4.5**), the relative yield of CO_2 compared to other products such as H_2O or benzenes is greater in PICA-D than the pure resin. Diphenyl ether is also released in region 3, after ether bond forming condensation, and this diphenyl ether yield is more significant in PICA-D than pure resin, again indicating increased condensation reactions. Methylene bridge scission reactions increase in region 3 as seen by the release of phenol groups, followed by the peak in CH_4 production from demethylation (**Figure 3.9**). Cresol has the highest yield out of the phenol species, followed by phenol, dimethyl phenol, and finally trimethyl phenol. In pure phenolic resin, phenol has the greatest yield compared to other methylated phenols, whereas in PICA-D cresol has the greatest yield, indicating increased cross linking in the resin of PICA-D. Additionally, trimethyl phenol is almost nonexistent in the yields from pure resin, and on the order of the molar yields of benzenes in PICA-D (see Appendix B **Figure A.B.2**). There is a large difference in the relative yields of scission products between pure resin and PICA-D, with the latter being smaller compared to other products such as light gases. This is again from increased crosslinking and condensation reactions within the resin phase or between the resin and carbon fibers leading to more thermally stable bonds in PICA-D. Xylene, toluene, and benzene are also formed after dehydroxylation of phenolic OH groups (**Figure 3.9**), or methylene bridge scission after the decomposition of ether bonds.

Unlike pure phenolic resin, some remaining methylene bridge scission reactions occur in region 4 for PICA-D, resulting in the production of some cresol. CH_4 continues to be produced from demethylation, and some from the decomposition of aromatic rings as seen by Yamashita and Ōuchi.[25] There is no additional bump in H_2O formation, indicating phenolic OH dehydroxylation is not a dominant process. This is likely because there is no H_2 pressure build up like in pure resin, and that most of the phenolic OH groups have already reacted through condensation reactions. CO

is continued to be produced from some ether bond condensation reactions, and now also from OH bonds remaining in the polycyclic aromatic hydrocarbons as reported by Kundu et. al.[38], with a proposed mechanism shown in **Figure 3.11**. Carbonization peaks in this region, signified by the peak of H_2 production. More H_2 is released in PICA-D relative to other yields as compared to the pure resin. This is because the H_2 produced easily escapes out of the porous material with little time for secondary reactions, and that some carbonization is also occurring in the carbon fibers to produce H_2 (**Figure 4.5**).

In region 5, there is no longer any methylene bridge scission and release of aromatic groups. There is the production of CO, from the decomposition of more stable complex ethers such as xanthene and benzofuran (**Figure 3.12**). Compared to pure phenolic resin, CO in this region may also originate from carbonyl, quinone, or ether groups in the FiberForm, as shown from pure FiberForm pyrolysis (**Figure 4.5**). H_2 continues to be produced with increasing carbonization. More relative CO is formed than in pure resin, from increased condensation and oxidized groups in the FiberForm. Very small amounts of H_2 is formed at 1200 °C, indicating near complete carbonization.

4.4 Temperature Gradient Dependencies

Figures 4.2 and **4.3** show the plots of mass and molar yields as a function of temperature for the temperature gradients of 1.08, 3.14, 5.92, 12.55, and 24.67 °C s^{-1} with the five different regions of decomposition indicated. With increasing temperature gradient, the most significant change that can be seen is a shift in regions to higher temperatures and slight broadening in production of yields across temperatures as residence time at each temperature decreases, as

described in Section 4.2. Trends do not change as drastically as in pure resin experiments, because of the low density increasing thermal and mass diffusion rates.

In region 1, the release of H_2O from chemisorption to carboxylic acid groups or reaction of two carboxylic acid groups shifts to higher temperatures. The CO_2 and propanol yields barely change. The products in region 1 shift around 75 °C in temperature from the lowest to highest temperature gradient. In region 2, the most significant change is the slight decrease in yield of H_2O, from the decrease in carbon-carbon bond forming condensation reactions. The production of CO and CH_4 do not appear to change much with increasing temperature gradient, except for at the highest temperature gradient where CO production in region 2 begins to blend in with region 3 (see Appendix B **Figure A.B.1**). This could be from diffusion effects, because CO is the heaviest product in region 2, and therefore would take the longest to diffuse out of the sample.[40]

Region 3 also does not change drastically with increasing temperature gradient, unlike pure resin. One consistency with the pyrolysis of pure phenolic resin is the decrease in production of CO_2 with the increase in temperature gradient, which is attributed to the decrease in H_2O production and shorter residence times preventing secondary reactions which form carboxylic acid groups and subsequently decomposition to CO_2. CO_2 is also still produced from the decomposition of carboxylic anhydrides in the FiberForm as discussed in section 4.3, leading to a much greater yield of CO_2 in PICA-D than pure resin, and because the formation of these anhydrides in region 1 indicated by the H_2O production appears not to change, it is possible a stable amount of CO_2 from the decomposition of carboxylic anhydrides is released at all temperature gradients. Slow ether bond forming condensation reactions also decrease slightly in region 3, similar to pure phenolic resin, and can be seen by the decrease in diphenyl ether production. Unlike pure phenolic

resin, the sum of all aromatic products peak at the temperature gradient of 3.14 °C s^{-1}, and then decreases slightly with an increasing temperature gradient, indicating scission reactions are not

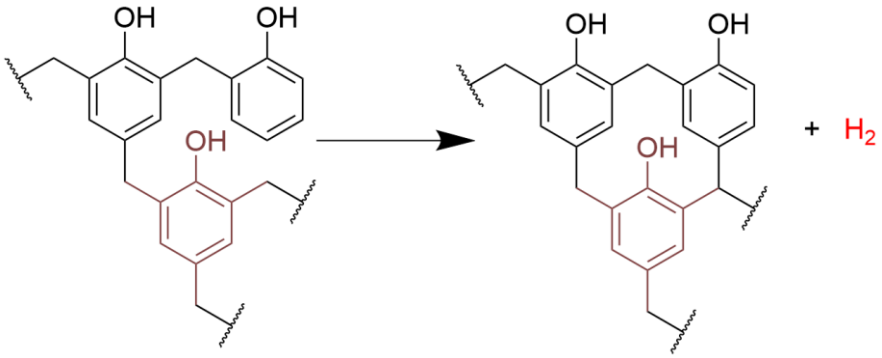

Figure 4.7 Carbon-carbon bond forming carbonization reaction within the backbone resin structure releasing H_2.

increasing with increasing temperature gradient. Also, the ratio of H_2 to volatile aromatics (**Figure 4.4**) decreases with increasing temperature gradient, possibly indicating a competition between methylene bridge scission and rapid carbonization. This is supported by the observation of a decrease in trimethyl phenol with increasing temperature gradient, with normalized molar yields decreasing from $3.19 - 1.89 \times 10^{-3}$, as it is the least probable phenol derivative to be produced because it requires the scission of three methylene bridges instead of one or two. Alternately, these bridges may form rings and release H_2 as shown in **Figure 4.7**. Trimethyl phenol is already a very minor product in the decomposition of pure phenolic resin, indicating that there is less initial crosslinking, or that there is already the influence of H_2 promoted scission even at the lowest temperature gradients, therefore this mechanism is not relevant for pure resin. In the pure phenolic resin, internal pressure buildup of H_2 increases with temperature gradient, and promotes methylene bridge scission. With the low density of PICA-D (~ 10 times lower than pure resin) this phenomenon does not occur, as gaseous products can easily make their way out of the structure without being forced to react. Since the yield of aromatic products decreases slightly, the dynamics

for the competition between condensation and methylene bridge scission of PICA-D are different than those of the pure solid resin. Because internal spatial thermal gradients are small for PICA-D, it is likely that condensation reactions and methylene bridge scission reactions do not compete as much, and instead the slow condensation reactions just decrease naturally as residence time at each temperature decreases. Condensation reaction may also decrease more readily in pure phenolic resin due to the possibility that steric effects may need to be overcome.

In region 4, H_2 production peaks, and with increasing temperature gradient shifts to higher temperatures, starting at around 640 °C at the lowest temperature gradient, and around 740 °C at the highest temperature gradient. Other than shifting and broadening across temperature slightly, the yields in region 4 do not change significantly.

The yields in region 5 visually appear to change the most with increasing temperature gradient. The larges change is the decrease in production of CO with increasing temperature gradient. This was observed by Bessire and Minton, and now also seen in both PICA-D and pure resin and is a result of the decreasing condensation reactions that lead to complex ethers such as xanthene and dibenzofuran.[8] H_2 continues to trail off at all temperature gradients to roughly baseline, indicating complete carbonization at all temperature gradients, unlike pure resin, likely a result of decreased spatial thermal gradient.

4.5 Comparison with Previous Work on PICA

Molar and mass yields along with synthesized TGA curves for the pyrolysis of PICA at four temperature gradients of 3.1, 6.1, 12.7, and 25.0 °C s^{-1} were previously collected in the experiment of Bessire and Minton[8], and led to great insight into the decomposition mechanism.

Improvements made to the experimental methodology and the recent study of pure SC-1008 resin allowed for increased accuracy in data and additional insights into the mechanisms. Now, with the new study of PICA-D, the extent to which the previous explanation of PICA decomposition is accurate can be determined. First, the previous synthesized TGA curves appear to contain effects from thermal gradients (20% lower temperature at edges compared to the center) and temperature measurement lag, resulting in broad temperature range of mass loss, and no capture of the shift to higher temperature with increased temperature gradient, a well-known trend in traditional TGA.[14,15,18]

When comparing yields at low temperatures, there is much more outgassing of H_2O in the previous PICA results from the absence of a standard post cure procedure. Also, the formation of CO_2 was greater, likely because in the current experiment there are not as many carboxylic acid groups as some would decompose during the post cure. As temperature increases, moving into region 2, two key differences are the lack of a distinct first peak in the H_2O and CO yields in previous results. For H_2O, this is likely the result of outgassing obstructing the distinctions, or from thermal gradients causing pyrolysis to happen at different stages across the sample. For CO, this is likely the result of a higher degree of initial oxidized species, such as ketones, yielding more CO in region 2 and then blending into region 3. The lack of distinct peaks in yields may also be from thermal gradients causing pyrolysis to happen at different stages across the sample. In regions 3 and 4, aside from slight differences in the temperatures at which products evolve and the width, the order of evolution of the previous PICA lines up with the new PICA-D data. The most significant difference is the H_2 yield, whose peak is much greater in the new data. This could be because H_2 is a difficult molecule to detect, therefore, it could easily be under accounted for. With the new experimental approach having a well-defined flux, and short distance between the sample

and detector ionizer, H_2 production is more accurately captured. In region 5, there are again differences in the H_2 yield, where the new data does not really show a bump in H_2 yields, and trails off to baseline indicating complete carbonization. This bump observed in the previous data at low temperature gradients was proposed to be a manifestation of the competition between condensation and methylene bridge scission reactions, however, as it is not observed even in the new data on pure phenolic resin, this reasoning is unlikely. Instead, this could have been an artifact from the large thermal gradient across the sample.

Though most of the previously proposed mechanisms by Bessire and Minton hold up when analyzing the new data, additional insight can be gained.[8] Aside from the improved fidelity of the data which revealed new details in the temperature-dependent product yields, 3 key new mechanistic details were found. First, one of the most significant contributions to the understanding of the decomposition was the identification of condensation reactions between oxidized species on FiberForm and the resin, which explain the high yields of CO and H_2O, and lower yields of methylene bridge scission products, compared to pure resin decomposition. The second new insight into the decomposition is that competition between condensation and methylene bridge scission is not a dominant mechanism when spatial thermal gradients are small, and when the material is porous. Instead, if heat transfer is fast and products can diffuse quickly out of the sample, these two reaction mechanisms do not appear to compete. Ether bond forming condensation reactions which lead to xanthene and dibenzofuran functional groups do decrease, as shown by the decrease in CO production at high temperatures, however, there are still enough ether bond condensation reactions occurring which produce quite a lot of CO and H_2O at all temperature gradients. Also, for PICA-D, the yield of aromatics does not increase with increasing temperature gradient, therefore methylene bridge scission is not significantly out competing

condensation. Instead, in these porous carbon phenolic materials, it is possible that methylene bridge scission begins to compete with rapid carbonization at high temperature gradients, as seen by the increasing ratio of H_2 to all aromatics. This increase was also seen by Bessire and Minton at the highest temperature gradient.[8] The final important new mechanistic insight is that to the first order, there is not much change in the temperature dependent relative yields at different temperature gradients, aside from shifting to higher temperatures, and the decrease in xanthene and benzofuran form condensation reactions. Further kinetics analysis needs to be performed to validate this claim.

4.6 Conclusion

Mass and molar yields of the 15 pyrolysis products have been identified for PICA-D as a function of five temperature gradients, 1.08, 3.14, 5.92, 12.55, and 24.67 °C s^{-1}, and have been compared with the yields of pure SC-1008 phenolic resole resin at similar temperature gradients to develop a greater understanding of the decomposition mechanism of carbon-phenolic composites. Unlike the previous results on pure SC-1008 resin and PICA[8], the temperature dependent yields do not show a strong temperature gradient dependence, indicating the mechanism of decomposition is significantly dominated by non-equilibrium processes as previously thought. The decreasing residence time at each temperature does cause a shift to higher temperatures with increasing temperature gradient as a result of diffusion, however, this shift is not nearly as significant as for the dense pure phenolic resin. Because PICA-D is porous and conductive, thermal gradients within the sample are not significant, resulting in reduced broadening across temperatures in the molar yield curves with increasing temperature gradient. With the reduced thermal nonequilibrium and lack of pressure buildup within the sample, the chemistry of

decomposition is also more in equilibrium, resulting in no clear competition between condensation and methylene bridge scission. Instead, aromatic products from methylene bridge scission are seen to decrease slightly with increased temperature gradient, indicating the mechanism favors carbonization. This also further proves that the increase in internal H_2 pressure build up in dense samples promotes methylene bridge scission with increasing temperature gradient. Xanthene and benzofuran forming condensation reactions do decrease, as predicted by Bessire and Minton, and is manifested by the decrease in CO production at high temperatures.[8] The current study, in conjunction with results from pure phenolic resin and mechanistic insight on the decomposition of PICA, has shown that oxidized species in FiberForm play an important role in increasing condensation reactions, which in turn increases the yield of H_2O and CO relative to the methylene bridge scission products, phenols and benzenes. The new results for the pyrolysis of PICA-D demonstrate how complex the decomposition of a carbon-phenolic system can be, showing that it depends on density, degree of oxidation of the carbon component, and possibly from what polymer the carbon component was derived. Reducing sample size and reducing temperature uncertainty has shown that the decomposition mechanism of PICA-D is not dominated by non-equilibrium process as previously observed, which may help reduce the complexity of modeling this system.

Chapter 5

Pyrolysis of 3MDCP-IL

Carbon-phenolic composites used in pyrolyzing ablative heat shields can be constructed with different densities, ratios of carbon to phenol, or different macroscale properties such as involving woven or felt-like carbon fiber, all to design a heat shield that will survive atmospheric entry conditions. Depending on the trajectory, atmosphere composition, and atmospheric density, the total heat flux a heat shield is required to absorb changes. For example, shallow trajectories subject the heat shield to the lowest temperature gradients, however the overall total heat flux absorbed is greater than for steep trajectories.[47] For the purpose of more extreme entry environments, NASA has developed a series of 3D woven carbon-phenolic composites under the name HEEET (heatshield for extreme entry environment technology).[48] One such material derived from HEEET technology is 3MDCP-IL (3D medium density carbon phenolic – insulation layer). 3MDCP-IL is composed of woven polyacrylonitrile derived carbon fibers, woven kynol phenolic resin fibers, and impregnated with SC-1008 resin. To understand how this new material pyrolyzes and allow for models to accurately capture its thermal response, data on the pyrolysis products and decomposition mechanisms of 3MDCP-IL is needed. To accomplish this, high fidelity data on the temperature dependent pyrolysis products for 3MDCP-IL has been collected at five linear temperature gradients with respect to time (0.95, 2.55, 5.52, 9.59, and 21.90 °C s^{-1}) using a method that was previously used to study the pyrolysis of two other phenolic compounds. Absolute and normalized molar and mass yields of 16 gaseous products (including N_2) have been determined as

a function of temperature, and thermogravimetric analysis (TGA) curves have been synthesized from the absolute mass yields. The yields and TGA curves exhibit temperature gradient dependencies more significant than PICA-D, but not as significant as seen with pure SC-1008 resin because of the differences in density. Comparison of the yields of 3MDCP-IL with PICA-D and pure resin led to the identification of interactions via additional condensation reactions occurring in both 3MDCP-IL and PICA-D between the resin and oxidized species on the carbon fibers, and identification of the production of N_2 from the polyacrylonitrile derived fibers in 3MDCP-IL. This new high-fidelity data has further proven that the density of the material, curing procedures, and whether or not carbon is present all have an effect on pyrolysis mechanisms of phenolic resin. This study has also shown that the from what polymer the carbon fibers were derived may contribute to additional products.

5.1 Experiment and Results

Experimental setup, procedures, and data analysis were performed as described in **Chapter 2**, for the pyrolysis study of 3MDCP-IL at five temperature gradients. The synthesized TGA curves (**Figure 5.1**), and molar (**Figure 5.2**) and mass yields (**Figure 5.3**) were used in conjunction with data and mechanisms from literature to identify the decomposition pathway, and how it changes with increasing temperature gradients, and the contributions of the carbon fibers.

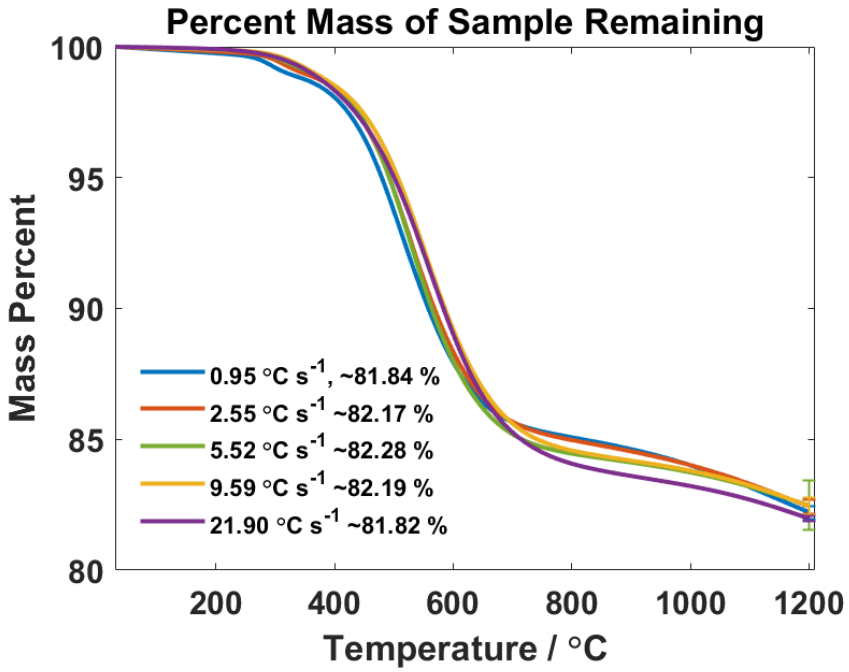

Figure 5.1 TGA curves synthesized from temperature-dependent mass for 16 compounds that evolved from 3MDCP-IL during pyrolysis with five different temperature gradients, as shown in the legend. The percentages of mass loss at the end of each run (i.e., 1200 °C) are also shown in the legend.

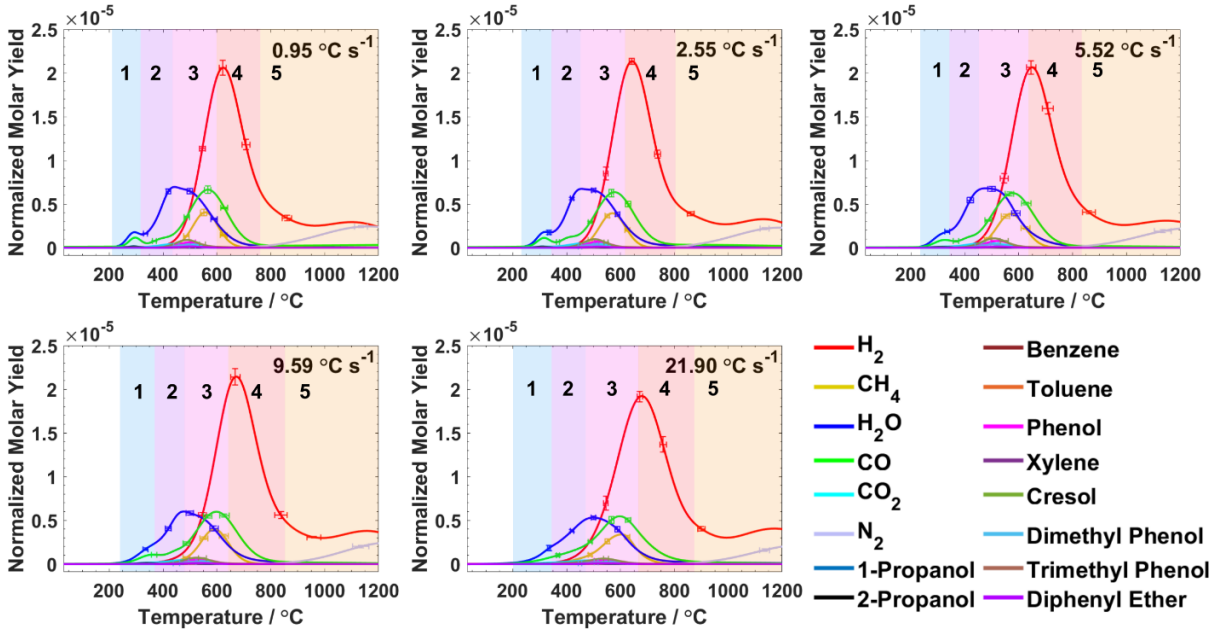

Figure 5.2 Temperature dependence of the molar yields of each gaseous pyrolysis compound normalized to the total molar yield of the 16 principal compounds that are assumed to evolve from3MDCP-IL during pyrolysis with five different temperature gradients, as indicated on each plot. Error bars represent ± 1σ for the five runs. Expanded plots excluding some high yield products are shown in Appendix C **Figures A.C.1 and A.C.2.**

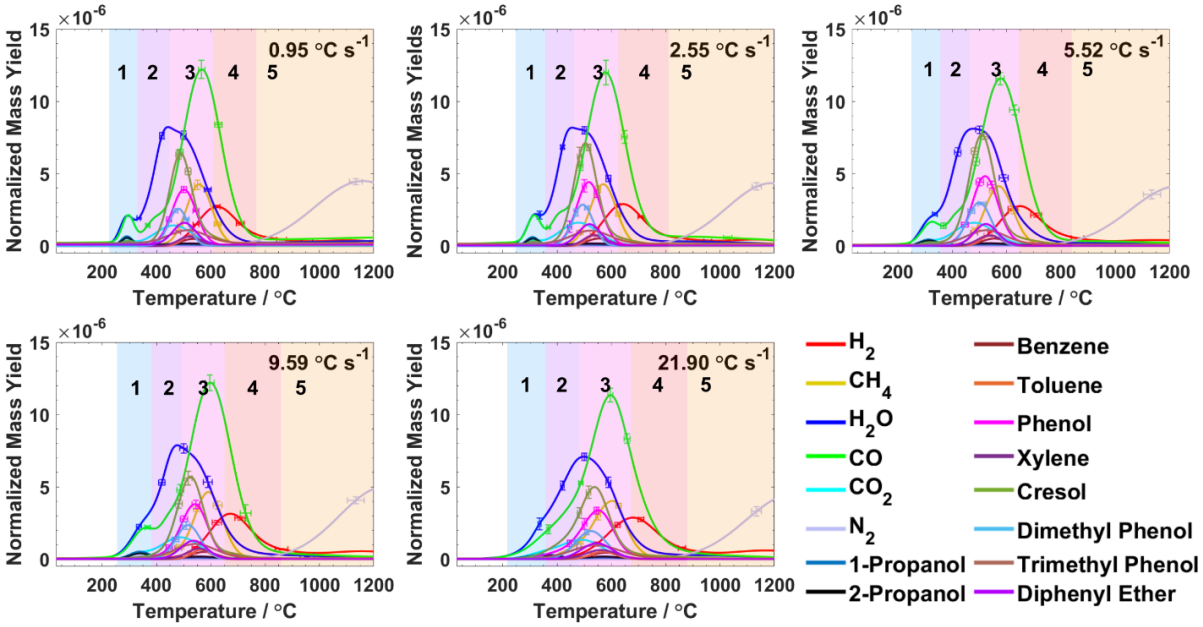

Figure 5.3 Temperature dependence of the mass yields normalized to the average total mass loss of 16 compounds that are assumed to evolve from 3MDCP-IL during pyrolysis with five different temperature gradients, as indicated on each plot. Error bars represent ±1σ from the five runs. Main regions of decomposition are identified by color and number.

5.2 Discussion of TGA Phenomena

The synthesized TGA (**Figure 5.1**) shows an initial mass loss between 300 – 400 °C, some shifting to higher temperatures and broadening of mass loss across temperatures with increasing temperature gradient, and indication for the continued decrease in mass loss above the temperature of 1200 °C. The initial dip in mass loss is a result of the release of H_2O and formaldehyde, which will be discussed in section 5.3. The TGA curves shifting to the right with increasing temperature gradient is a well-known trend seen in TGA data, and is a result of the shortening residence time at each temperature with increased temperature gradient.[14,15,18] The shortening residence time may affect the reaction extent at each temperature and the diffusion rate, which both lead to a delay or increase in the temperature at which a specific product is observed. The shortening of residence time may also affect temperature uniformity, as temperature gradients become on the order of or faster than heat conduction rates. The heat conduction in 3MDCP-IL is important to consider for two reasons; (1) at these sample sizes the material is not solid and may not be in uniform contact with the FiberForm sample holder, and (2), the thermal conductivity is not uniform as a result of the weave, which has been shown in modeling experiments by Askins et. al.[49] Both these properties introduce temperature nonuniformity, leading to the broadening in distribution of products and mass loss. Because 3MDCP-IL is porous, products do not require much diffusion time through the material before being detected, therefore this temperature nonuniformity does not result in much shifting of products to higher temperatures like solid samples such as pure SC-1008, and instead only broadens the distributions. The samples are large enough that the broadening begins to compete with the natural shift to higher temperatures from reduced residence time, leading to very little distinction between shifting of each temperature gradient. If the sample was even larger and had greater temperature nonuniformity, this distinction between shifting from reduced residence

time and broadening in mass loss from temperature nonuniformity may even result in a shifting to lower temperatures with increased temperature gradient, as observed by Bessire and Minton.[8]

The observation of mass loss continuing to increase at 1200 °C is from the production of N_2 and H_2 from the polyacrylonitrile derived carbon-fibers.[50] According to Mittal et. al., weight loss of PAN fibers is seen up to temperatures of 1900 °C and is from the release of N_2 and H_2, where H_2 formation stops before N_2 formation at 1500 °C.[51]

Similar to PICA-D, 3MDCP-IL does not show a distinct increase in mass loss with increasing temperature gradient, unlike pure SC-1008 resin. This could be a result of three factors; (1) nonuniformity between samples, (2) errors in mass loss measurements, (3) increased probability for crosslinking reactions. First, these samples may be more nonuniform than PICA-D because the weave structure is on a larger scale than the fibers in FiberForm. 3MDCP-IL also contains very fine fibers of carbon and phenol that easily get stuck to the FiberForm holder, resulting in a large standard deviation in mass loss measurements. The main reason though is the increase in probability for condensation reactions between the resin and oxidized species on the carbon fibers, which decreases the likelihood of methylene bridge scission reactions that lead to mass loss, masking the effect of condensation vs methylene bridge scission reactions.

5.3 Temperature-Dependent Decomposition Mechanism

Similar to previous work, the temperature dependent decomposition of 3MDCP-IL can be split up into 5 main regions as seen in **Figures 5.2 and 5.3**. The general mechanism and decomposition products arising from the pyrolysis of the resin in the composite is the same, however, differences arise in the overall temperature-dependent yields as a result of the different

density, curing procedures, interactions with the carbon fibers, and source of the carbon fibers. In region 1, some outgassing of likely residual solvents 1-propanol and 2-propanol is observed, as well as H_2O, CO, CO_2, and small amounts of phenol and cresol. H_2O may come from chemisorption or through the reactions of two carboxylic acid groups, likely present in the carbon fiber phase, which is the same as what occurs in region 1 for PICA-D.[43,44] H_2O may also come from the continuation of polymerization reactions. It appears that quite a significant yield of CO is formed in region 1, however, when examining the raw mass spectra carefully, the fragmentation pattern more closely matches that of formaldehyde, and not CO. This, in combination with the release of some phenol and cresol, suggests that the phenol-formaldehyde resin was not fully cured or that the two sources of resin (kynol fibers and impregnation of SC-1008 resin) were cured differently. The small amounts of CO_2 result from the decomposition of carboxylic acid groups that were present, and that did not react to form carboxylic anhydrides, matching observations with PICA-D. H_2O is formed from the reaction of two adjacent carboxylic acid groups to form carboxylic anhydrides (**Figure 4.6**). There is a greater relative yield of CO_2 and H_2O in region 1 for 3MDCP-IL as compared to PICA-D, indicating increased initial oxidation and presence of carboxylic acid groups.

Region 2 for 3MDCP-IL behaves similar to region 2 for PICA-D, where the main products are H_2O, CO, and CH_4. Methylene bridge scission also begins to occur towards the end of region 2, as seen by the start of release of phenol and derivatives. H_2O is released after carbon-carbon bond forming condensation reactions within the resin structure and between the resin and carbon fibers. CO is formed after dehydrogenation of residual methylol groups in the resin, and subsequent decomposition,[8] or from the decomposition of ketone groups like benzophenone, which were formed after oxidation of methylene bridges and may be present in the virgin material,

or formed after oxidation by the produced H_2O.[28] In region 2, H_2O may also react after dehydrogenation of a methylol group to form carboxylic acid.

The primary reaction in region 3 is the formation of ether bonds through condensation reactions, either within the resin or between the resin and oxidized species on the carbon fibers, releasing H_2O as a product.[41] A portion of H_2O may also be formed through dehydroxylation of phenolic OH groups. The majority of ether bonds formed subsequently decompose to produce CO. Similar to PICA-D, the relative yields of CO and H_2O are much greater than in the pure resin, because of the presence of oxidized species in the carbon fibers that facilitate an increase in ether bond forming condensation during the curing or pyrolysis processes. CO_2 is formed from the decomposition of carboxylic anhydrides formed in region 1, and from oxidized species formed from secondary reactions of H_2O. The relative yield of CO_2 is greater for 3MDCP-IL than PICA-D, indicating a higher degree of initial oxidation, and similar to PICA-D much greater than pure resin. Diphenyl ether is released in region 3 after the formation of ether bond forming condensation reactions.[8] Additionally, the relative yield of diphenyl ether is also greater than PICA-D, likely as a result of increased oxidation of the carbon fibers, leading to increased ether bond forming condensation reactions between the carbon fibers and resin. Methylene bridge scission reactions peak in region 3, leading to the production of phenol and derivatives, followed by CH_4 from demethylation. Like in PICA-D, cresol has the highest peak of the phenol species, followed by phenol, dimethyl phenol, and trimethylphenol. However, the ratio of phenol compared to methylated phenols is greater for 3MDCP-IL than PICA-D, indicating a lesser degree of crosslinking. Both 3MDCP-IL and PICA-D have higher degrees of crosslinking than the pure resin, whose primary phenol product was phenol. Small amounts of xylene, toluene, and benzene

are produced in region 3 from scission after the decomposition of ether bonds or dehydroxylation of phenolic OH groups.

In region 4, H_2 production peaks, and CO, CH_4, and H_2O continue to be produced. Because the material is porous, internal H_2 pressure does not increase, and therefore no additional bump in H_2O production is observed, just like for PICA-D. In region 4, above 600 °C, HCN and NH_3 are known to be produced from the pyrolysis of PAN fibers.[52,53] These products were not observed in the mass spectral data on the pyrolysis of 3MDCP-IL, as $m/z = 17$ which corresponds to NH_3 and $m/z = 27$ which corresponds to HCN did not start to increase above 600 °C.

In region 5, the main products are H_2, N_2, and CO. H_2 is formed from carbonization reactions, and from the reaction of residual N-H groups as shown in Figure 5 reaction 1, as proposed by Watt.[54] According to Georgiou, N-H bond may be present in the cured novalac based resin from curing agents, as seen by the broader IR peak and shoulder at 1635 nm in novalac based carbon compared to resole based carbon.[55] Kynol is a novalac derived resin, therefore may contain N-H bonds. The additional source of H_2 production from the decomposition of N-H bonds may cause the bump in H_2 seen above 1000 °C for 3MDCP-IL, which is not seen in PICA-D. The significant molar yields of N_2 in region 5 are from the reaction of two sp^2 nitrogen atoms within the aromatic carbon fiber structure, as seen in **Figure 5.4** reaction 2.[50] N_2 is not produced in PICA-D because the carbon fibers of are not derived from a nitrogen containing polymer. Both N_2 and H_2 are still being produced at 1200 °C, indicating the reactions shown in **Figure 5.4** are ongoing. Finally, CO is produced in region 5 from the decomposition of more stable complex ethers such as xanthene and benzofuran, and possibly carbonyl, quinone, or ether groups present in the carbon fibers.

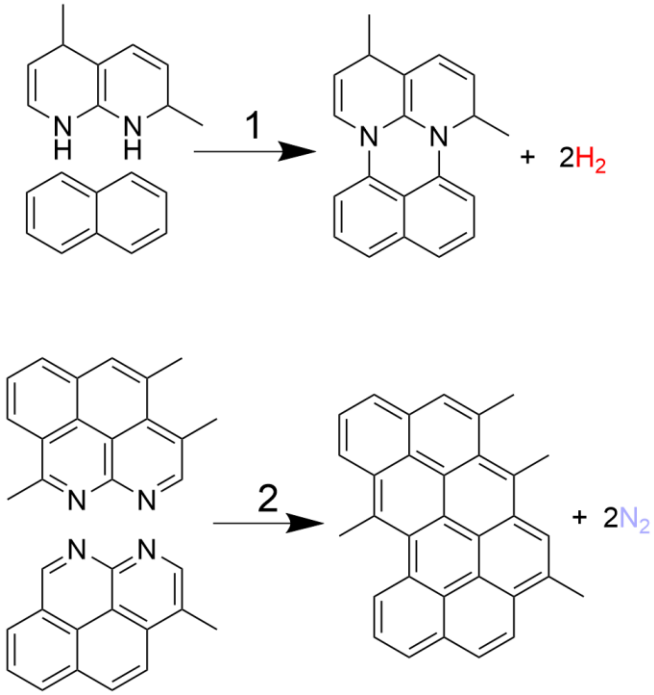

Figure 5.4 (1) Formation of H_2 from the reaction of N-H groups. (2) Formation of N_2 from the reaction of sp^2 nitrogen.

5.4 Temperature Gradient Dependencies

As seen in **Figures 5.2** and **5.3**, the normalized yields during the pyrolysis of 3MDCP-IL do change some with increasing temperature gradient. Similar to PICA-D, the yields shift to higher temperatures and yields broaden across temperatures with increasing temperature gradient, but do not change as drastically as pure resin as a result of the lower density and increased thermal and mass diffusion rates. However, the shifting and broadening for 3MDCP-IL is greater than PICA-D as a result of increased temperature nonuniformity of the larger, nonhomogeneous samples.

All products in region 1, the release of H_2O from chemisorption of reaction of two carboxylic acid group, release of possible formaldehyde and solvents, shift to higher temperatures and broaden with increasing temperature gradient. Similar behavior is seen in region 2, with

widening and shifting. Also in region two, there is a very slight decrease in the peak of H_2O formation from the decrease in slow carbon-carbon bond forming condensation reactions.

In region 3, the peak in yields of aromatic products such as phenols and benzenes decrease, as their observed yields broaden across temperatures as a result of temperature nonuniformity. This broadening in yields across temperatures is much more significant for 3MDCP-IL than PICA-D, because of greater spatial temperature nonuniformity. The production of CO_2 however does not change much in region 3, which could indicate that the majority of CO_2 is formed from the decomposition of carboxylic anhydrides formed on the carbon fibers, similar to PICA-D. The diphenyl ether yield from slow ether bond forming condensation reactions decrease, with increasing temperature gradients, as also seen for PICA-D and pure SC-1008. However, H_2O production does not change much and decreases at the two highest temperature gradients, indicating that internal H_2 pressure does not increase with increasing temperature gradient and therefore does not promote dehydroxylation of the phenolic OH bond, unlike pure resin. There may be, however, some competition between condensation and methylene bridge scission. This is seen by the decrease in ratio of H_2O and phenols and derivatives with increasing temperature gradient (**Figure 5.5**), and may be influenced by spatial temperature gradients, which were very minimal in PICA-D. This ratio increases at the highest temperature gradient however, and this is a result of the abrupt decrease in phenols and derivatives, and not the increase in H_2O from phenolic OH bond decomposition as like in pure resin. This matches the trend observed in PICA-D, where there was observed possible competition between methylene bridge scission and rapid carbonization, which would lead to a decrease in methylene bridge scission products at high temperature gradients. Similar to PICA-D, the yield of trimethyl phenol decreases with increasing

temperature gradient, as it is the least probable phenol derivative to be produced, and instead functionalities of trimethyl phenol may undergo carbonization reactions.

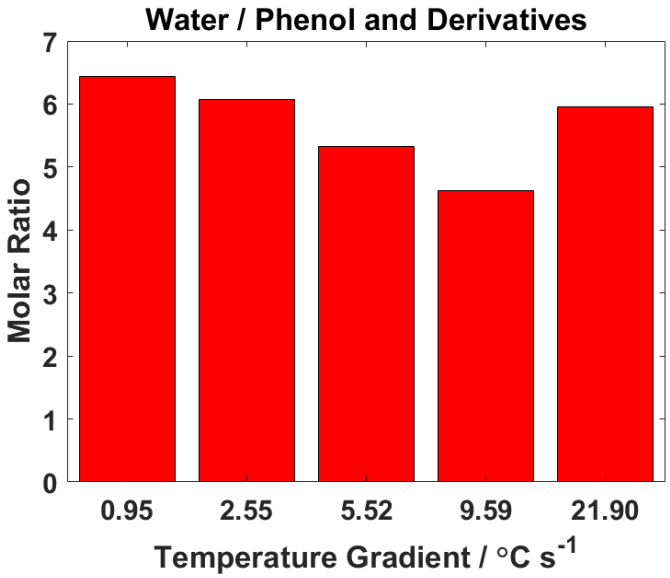

Figure 5.5 Ratio of integrated molar yield of H_2O to integrated molar yield of phenol and its derivatives for the temperature gradients of 0.95, 2.55, 5.52, 9.59, and 21.90 °C s^{-1}.

Region 4 does not change significantly other than shifting and broadening across temperatures. The broadening is greater than PICA-D, again because of temperature nonuniformity. The yields in region 5 also shift to higher temperatures with increased temperature gradient. The yield of H_2 in region 5 does not change much with increasing temperature gradient, but does appear to increase slightly. A possible reason for this is the competition between methylene bridge scission and carbonization, leading to increased carbonization with increased temperature gradient. N_2 yields decrease significantly with increasing temperature gradient, and shift to higher temperatures. This may be because as residence time at each temperature decreases, steric effects become more important and could hinder two sp^2 nitrogen groups from coming together and reacting through reaction 2 **Figure 5.4**.

5.5 Conclusion

Temperature dependent molar and mass yields of 16 pyrolysis products have been identified for 3MDCP-IL at five different temperature gradients, 0.95, 2.55, 5.52, 9.59, and 21.90 °C s^{-1}. These yields have been compared to yields of pure SC-1008 resin and PICA-D at similar temperature gradients to understand the effects of density, carbon fibers, and curing procedures. Like PICA-D, 3MDCP-IL shows evidence for interactions between oxidized species on the carbon fibers and resin, leading to the increase in condensation reactions which release H_2O and CO, and the decrease in methylene bridge scission reactions as compared to pure SC-1008 resin. This increase in condensation also resulted in the decreased effect of the competition between condensation and methylene bridge scission. The increased density compared to PICA-D, much larger sample sizes, and nonuniform thermal conductivity led to an increase in the broadening in production of pyrolysis products across temperatures compared to PICA-D and masked the shifting of yields to higher temperatures with increased temperature gradient. N_2 production from the PAN based carbon fibers was found to be released above 800 °C, and was still being produced at 1200 °C, leading to continued mass loss above 1200 °C. Similar to PICA-D and as a result of decreased density compared to pure resin, H_2 internal pressure did not build up and therefore did not promote dehydroxylation of OH groups with increasing temperature gradient. This novel work on the pyrolysis of 3MDCP-IL has shown how sample sizes, thermal conductivity and temperature nonuniformity, and from what polymer the carbon fibers are derived all effect the temperature gradient dependent decomposition of carbon-phenolic composites. With this data, it can be seen that the pyrolysis of 3MDCP-IL is a non-equilibrium process, with relative yields changing with increasing temperature gradient. However, the relative yields do not change as much as those of pure SC-1008 resin, because of the decreased density. The data obtained in conjunction with data

on PICA-D and SC-1008 has led to obtaining even more insight into the effects of thermal conductivity and uniformity, density, and carbon fibers on the pyrolysis of carbon-phenolic composites.

Chapter 6

Conclusion

In order to better understand the temperature dependent pyrolysis of phenolic resin and carbon-phenolic composites, a new apparatus, Pyrolysis 2.0, was assembled and calibrated, data analysis method developed, and experimental campaigns conducted on three different materials relevant to atmospheric entry heat shields: pure phenolic SC-1008 resin, PICA-D, and 3MDCP-IL. Mass and molar yields of 15 (or 16) pyrolysis products have been identified for these phenolic materials as they decomposed at 5 temperature gradients, across a temperature range of 25 to 1200 °C. TGA curves have been synthesized from the mass yields and total mass loss. The data was used in conjunction with literature data and known reactions to identify the temperature dependent pyrolysis mechanisms for each material, and identify the effects of temperature gradient, density, temperature nonuniformity, curing procedures, and carbon fibers. Both the molar yields and TGA curves for pure SC-1008 resin show a clear dependence on temperature gradient, therefore the pyrolysis of pure phenolic resin is a non-equilibrium process. The competition between reactions depended on the temperature gradient and caused the pyrolysis path to change. Condensation reactions occur relatively slowly and form thermally stable, carbon-preserving ether bonds, and at higher temperature gradients, methylene bridge scission outcompetes condensation and results in enhanced mass loss through the production of phenol and its derivatives with increasing temperature gradient. Increasing internal H_2 pressure which builds up in the dense material resulted in an increase in yields of H_2O, CO, and CH_4. With this baseline data on cured SC-1008 resin and comparison with data on carbon phenolic materials, insights were made into carbon/phenolic decomposition mechanisms. Different curing procedures lead to residual isopropanol solvent and

phenol released at lower temperatures for the cured resin that was not seen in the composites. Additional condensation reactions were identified between oxidized species on carbon fibers and the phenolic resin phase, leading to increased charr yields, decrease in production of volatile aromatics from methylene bridge scission, and increased production of H_2O and CO. This increase in condensation reactions resulted in no distinct competition between condensation and methylene bridge scission, and therefore no observable increase in mass loss with increasing temperature gradient. The origin of carbon fibers also affected yields; for example, the PAN derived fibers in 3MDCP-IL still produced N_2 at high temperatures. The identification of the contribution to pyrolysis products and reaction mechanisms from carbon fibers can help to determine what combination of carbon fibers and phenolic resin is ideal for certain atmospheric entry scenarios. The high-fidelity data and new understandings of the decomposition mechanisms of phenolic materials can be used to obtain kinetic parameters that can be applied to improving materials response models. The quantification of pyrolysis gases that subsequently travel into the boundary layer can help understand transport properties and be applied to boundary layer models. This data, insights, and improved models will lead to less discrepancies between models and flight data, resulting in better heat shield design and performance predictions.

Bibliography

(1) Anderson, J. D. *Hypersonic and High Temperature Gas Dynamics*; AIAA, 1989.

(2) Laub, B.; Venkatapathy, E. Thermal Protection System Technology and Facility Needs for Demanding Future Planetary Missions. In *International Workshop Planetary Probe Atmospheric Entry and Decent Trajectory Analysis and Science*, Lisbon, Portugal, October 6-9, 2003; Wilson, A.; ESA Publications Division: Noordwijk, Netherlands, 2004; Vol. 544, pp 239-247.

(3) Violette, M. S.; Sullivan, P. Development and Fabrication of Thermal Protection Systems for NASA: Enabling the Exploration of Our Solar System. In *AIAA SCITECH 2024 Forum*, Orlando, Florida, January 8-12, 2024; DOI: 10.2514/6.2024-0367

(4) Mahzari, M.; Braun, R. D.; White, T. R.; Bose, D. Inverse Estimation of the Mars Science Laboratory Entry Aeroheating and Heatshield Response. *J. Spacecr. Rockets* **2015**, *52* (4), 1203-1216. DOI: 10.2514/1.A33053

(5) Gosma, M. R.; Harper, C. N.; Collins, L. N; Stephani, K. A.; Engerer, J. D. Chemical Kinetics and Thermal Properties of Ablator Pyrolysis Products During Atmospheric Entry. *J. Thermophys. Heat Transf.* **2024**, Articles in Advance. DOI: 10.2514/1.T6921 (accessed 2024-12-19).

(6) Biordi, J. C. Molecular Beam Mass Spectrometry for Studying the Fundamental Chemistry of Flames. *Prog. Energy Combust. Sci.* **1977**, *3*(3), 151-173. https://doi.org/10.1016/0360-1285(77)90002-8.

(7) Hansen, N.; Cool, T. A.; Westmoreland, P. R.; Kohse-Höinghaus, K. Recent Contributions of Flame-Sampling Molecular-Beam Mass Spectrometry to a Fundamental Understanding of Combustion Chemistry. *Prog. Energy Combust. Sci.* **2009**, *35*(2), 168-191. https://doi.org/10.1016/j.pecs.2008.10.001.

(8) Bessire, B. K.; Minton, T. K. Decomposition of Phenolic Impregnated Carbon Ablator (PICA) as a Function of Temperature and Heating Rate. *ACS Appl. Mater. Interfaces* **2017**, *9*(25), 21422-21437. DOI: 10.1021/acsami.7b03919

(9) Bessire, B. K.; Lahankar, S. A.; Minton, T. K. Pyrolysis of Phenolic Impregnated Carbon Ablator (PICA). *ACS Appl. Mater. Interfaces* **2015**, *7* (3), 1383-1395. DOI: 10.1021/am507816f

(10) Bose, D.; Olson, M.; Laub, B.; White, T.; Feldman, J.; Santos, J.; Mahzari, M.; MacLean, M.; Dufrene, A.; Holden, M. In *51st AIAA Aerospace Sciences Meeting including the New Horizons*

Forum and Aerospace Exposition, Grapevine, Texas, January 7-10, 2013; DOI: 10.2514/6.2013-908

(11) Cohen, Y.; Aizenshtat, Z. Investigation of Pyrolytically Produced Condensates of Phenol-Formaldehyde Resins, in Relation to Their Structure and Decomposition Mechanism. *J. Anal. Appl. Pyrolysis* **1992**, *22* (3), 153-178. DOI: 10.1016/0165-2370(92)85010-I

(12) *Durite SC-1008*; MSDS No. 000000000244; Hexion Specialty Chemicals: Louisville, KY, February 25, 2010.

(13) Jeans, J. *The Dynamical Theory of Gases*; University Press, 1925.

(14) Bevis, J.; Bottom, R.; Duncan, J.; Farhat, I.; Forrest, M.; Furniss, D.; MacNaughton, B.; Nazhat, S.; Saunders, M.; Seddon, A. *Principles and Applications of Thermal Analysis*; Gabbott, P., Eds.; Wiley Online Library, 2008. DOI: 10.1002/9780470697702

(15) Seebauer, V.; Petek, J.; Staudinger, G. Effects of Particle Size, Heating Rate and Pressure on Measurement of Pyrolysis Kinetics by Thermogravimetric Analysis. *Fuel* **1997**, *76* (13), 1277-1282. DOI: 10.1016/S0016-2361(97)00106-3

(16) Nam, J.-D; Seferis, J. C. Initial Polymer Degradation as a Process in the Manufacture of Carbon-Carbon Composites. *Carbon* **1992**, *30* (5), 751-761. DOI: 10.1016/0008-6223(92)90158-S

(17) Wang, C. J. The Effects of Resin Thermal Degradation on Thermosctructural Response of Carbon-Phenolic Composites and the Manufacturing Process of Carbon-Carbon Composites. *J. Reinf. Plast. Compos.* **1996**, *15* (10), 1011-1016. DOI: 10.1177/073168449601501003

(18) Vyazovkin, S.; Chrissafis, K. Di Lorenzo, M. L., Koga, N.; Pijolat, M.; Roduit, B.; Sbirrazzuoli, N.; Suñol, J. J. ICTAC Kinetics Committee Recommendations for Collecting Experimental Thermal Analysis Data for Kinetic Computations. *Thermochim. Acta* **2014**, *590*, 1-23. DOI: 10.1016/j.tca.2014.05.036

(19) Stokes, E. H. Kinetics of Pyrolysis Mass Loss from Cured Phenolic Resin. *J. Thermophys. Heat Transf.* **1995**, *9* (2), 352-358. DOI: 10.2514/3.667

(20) Brunner, P. H.; Roberts, P. V. The Significance of Heating Rate on Char Yield and Char Properties in the Pyrolysis of Cellulose. *Carbon* **1980**, *18* (3), 217-224. 10.1016/0008-6223(80)90064-0

(21) Ros, T. G.; Van Dillen, A. J.; Geus, J. W.; Koningsberger, D. C. Surface Oxidation of Carbon Nanofibres. *Chem. Eur. J.* **2002**, *8* (5), 1151-1162. DOI: 10.1002/1521-3765(20020301)8:5<1151::AID-CHEM1151>3.0.CO;2-%23

(22) Morterra, C.; Low, M. J. D. IR Studies of Carbons—VII. The Pyrolysis of a Phenol-Formaldehyde Resin. *Carbon* **1985**, *23* (5), 525-530. DOI: 10.1016/0008-6223(85)90088-0

(23) Ōuchi, K. Infra-Red Study of Structural Changes during the Pyrolysis of a Phenol-Formaldehyde Resin. *Carbon* **1966**, *4* (1), 59-66. DOI: 10.1016/0008-6223(66)90009-1

(24) Trick, K. A.; Saliba, T. E. Mechanisms of the Pyrolysis of Phenolic Resin in a Carbon/Phenolic Composite. *Carbon* **1995**, *33* (11), 1509-1515. DOI: 10.1016/0008-6223(95)00092-R

(25) Yamashita, Y.; Ōuchi, K. A Study on Carbonization of Phenol-Formaldehyde Resin Labelled with Deuterium and 13C. *Carbon* **1981**, *19* (2), 89-94. DOI: 10.1016/0008-6223(81)90112-3

(26) Blanksby, S. J.; Ellison, G. B. Bond Dissociation Energies of Organic Molecules. *Acc. Chem. Res.* **2003**, *36* (4), 255-263. DOI: 10.1021/ar020230d

(27) Rossi, M. J.; McMillen, D. F.; Golden, D. M. Aliphatic Carbon-Hydrogen Bond Scission Processes in Diphenylmethane and 2-Benzyl- and 4-Benzylpyridine. The Heat of Formation of the Diphenylmethyl and α-Phenylethyl Radical in the Gas Phase. *J. Phys. Chem.* **1984**, *88* (21), 5031-5039. DOI: 10.1021/j150665a048

(28) Conley, R. T.; Bieron, J. F. A Study of the Oxidative Degredation of Phenol-Formaldehyde Polycondensates Using Infrared Spectroscopy. *J. Appl. Polym. Sci.* **1963**, *7* (1), 103-117. DOI: 10.1002/app.1963.070070110

(29) Torres-Herrador, F.; Eschenbacher, A.; Coheur, J.; Blondeau, J.; Magin, T. E.; Van Geem, K. M. Decomposition of Carbon/Phenolic Composites for Aerospace Heatshields: Detailed Speciation of Phenolic Resin Pyrolysis Products. *Aerosp. Sci. Technol.* **2021**, *119*, 107079. DOI: 10.1016/j.ast.2021.107079

(30) Shulman, G. P.; Lochte, H. W. Thermal Degradation of Polymers. II. Mass Spectrometric Thermal Analysis of Phenol-formaldehyde Polycondensates. *J. Appl. Polym. Sci.* **1966**, *10* (4), 619-635. DOI: 10.1002/app.1966.070100407

(31) Parker, J. A.; Winkler, E. L. *The Effects of Molecular Structure on the Thermochemical Properties of Phenolics and Related Polymers*; National Aeronautics and Space Administration, 1967.

(32) Robichaud, D. J.; Nimlos, M. R.; Ellison, G. B. Pyrolysis Mechanisms of Lignin Model Compounds Using a Heated Micro-Reactor. In *Reaction Pathways and Mechanisms in Thermocatalytic Biomass Conversion II*; Schlaf, M.; Zhang, Z. C., Eds.; Springer Singapore, 2016; pp 145-171. DOI: 10.1007/978-981-287-769-7_8

(33) Bennett, A.; Payne, D.; Court, R. Quantitative Pyrolytic and Elemental Analysis of Phenolic Resin. In *51st AIAA Aerospace Sciences Meeting including the New Horizons Forum and Aerospace Exposition*, Grapevine, Texas, January 7-10, 2013; DOI: 10.2514/6.2013-183

(34) Jones, B. W.; Neuworth, M. B. Thermal Cracking of Alkyl Phenols – Mechanism of Dealkylation. *Ind. Eng. Chem.* **1952**, *44* (12), 2872-2876. DOI: 10.1021/ie50516a034

(35) Buryan, P. Thermal Decomposition of Dimethylphenols. *J. Anal. Appl. Pyrolysis* **1991**, *22* (1), 83-93. DOI: 10.1016/0165-2370(91)85008-U

(36) Patel, P.; Hull, T. R.; McCabe, R. W.; Flath, D.; Grasmeder, J.; Percy, M. Mechanism of Thermal Decomposition of Poly (Ether Ether Ketone)(PEEK) from a Review of Decomposition Studies. *Polym. Degrad. Stab.* **2010**, *95* (5), 709-718. DOI: 10.1016/j.polymdegradstab.2010.01.024

(37) Day, M.; Cooney, J. D.; Wiles, D. M. The Thermal Degradation of Poly (Aryl—Ether—Ether—Ketone)(PEEK) as Monitored by Pyrolysis—GC/MS and TG/MS. *J. Anal. Appl. Pyrolysis* **1990**, *18* (2), 163-173. DOI: 10.1016/0165-2370(90)80005-9

(38) Kundu, S.; Wang, T.; Xia, W.; Muhler, M. Thermal Stability and Reducibility of Oxygen-Containing Functional Groups on Multiwalled Carbon Nanotube Surfaces: A Quantitative High-Resolution XPS and TPD/TPR Study. *J. Phys. Chem. C* **2008**, *112* (43), 16869-16878. DOI: 10.1021/jp804413a

(39) Figueiredo, J. L.; Pereira, M. F. R.; Freitas, M. M. A.; Orfao, J. J. M. Modification of the Surface Chemistry of Activated Carbons. *Carbon* **1999**, *37* (9), 1379-1389. DOI: 10.1016/S0008-6223(98)00333-9

(40) Berens, A. R.; Hopfenberg, H. B. Diffusion of Organic Vapors at Low Concentrations in Glassy PVC, Polystyrene, and PMMA. *J. Membr. Sci.* **1982**, *10* (2-3), 283-303. DOI: 10.1016/S0376-7388(00)81415-5

(41) Ko, T. H. The effect of pyrolysis on the mechanical properties and microstructure of carbon fiber-reinforced and stabilized fiber-reinforced phenolic resins for carbon/carbon composites. *Polymer Composites* **1993**, *14*(3), 247-256. DOI: 10.1002/pc.750140310

(42) Yang, Z.; Liu, B.; Zhao, H.; Li, J.; Guo, X.; Zhang, D. ; Liu, Z. Pyrolysis Mechanism of Composite Binder Composed of Coal Tar Pitch and Phenolic Resin for Carbon Materials. *J. Anal. Appl. Pyrolysis* **2023**, *169*, 105840. DOI: 10.1016/j.jaap.2022.105840

(43) Zeng, Y.; Xu, H.; Horikawa, T.; Do, D. D.; Nicholson, D. Henry Constant of Water Adsorption on Functionalized Graphite: Importance of the Potential Models of Water and Functional Group. *J. Phys. Chem. C* **2018**, *122* (42), 24171–24181. DOI: 10.1021/acs.jpcc.8b08036

(44) Rosillo-Lopez, M.; Lee, T. J.; Bella, M.; Hart, M.; Salzmann, C. G. Formation and Chemistry of Carboxylic Anhydrides at the Graphene Edge. *RSC Adv.* **2015**, *5* (126), 104198–104202. DOI: 10.1039/C5RA23209K

(45) Cabrera, A. L.; Heinemann, H.; Somorjai, G. A. Methane production from the catalyzed reaction of graphite and water vapor at low temperatures (500-600 K). *J. Catala.***1982**, *75* (1), 7-22. DOI: 10.1016/0021-9517(82)90117-8

(46) Chen, C. M.; Zhang, Q.; Yang, M. G.; Huang, C. H.; Yang, Y. G.; Wang, M.-Z. Structural Evolution during Annealing of Thermally Reduced Graphene Nanosheets for Application in Supercapacitors. *Carbon* **2012**, *50* (10), 3572–3584. DOI: 10.1016/j.carbon.2012.03.029

(47) Chapman, D. R. *An Approximate Analytical Method for Studying Entry Into Planetary Atmospheres*; U.S. Government Printing Office, 1959.

(48) Stackpoole, M.; Ellerby, D.; Gasch, M.; Venkatapathy, E. Thermal Protection System Technology Maturation and Sustainment in Support of In Situ Science Missions: HEEET and PICA. In *Ablation Workshop* 2019.

(49) Askins, P.; Martin, A.; Libben, B.; Palmer, G.; William, J. Semi-emperical 1d material response modeling using inverse methods. In *AIAA AVIATION 2022 Forum* 2022.

(50) Laffont, L.; Monthioux, M.; Serin, V.; Mathur, R. B.; Guimon, C.; Guimon, M. F. An EELS Study of the Structural and Chemical Transformation of PAN Polymer to Solid Carbon. *Carbon* **2004**, *42* (12), 2485–2494. DOI: 10.1016/j.carbon.2004.04.043

(51) Mittal, J.; Konno, H.; Inagaki, M.; Bahl, O. P. Denitrogenation Behavior and Tensile Strength Increase during Carbonization of Stabilized Pan Fibers. *Carbon* **1998**, *36* (9), 1327–1330. DOI: 10.1016/S0008-6223(98)00113-4

(52) Rahaman, M. S. A.; Ismail, A. F.; Mustafa, A. A Review of Heat Treatment on Polyacrylonitrile Fiber. *Polym. Degrad. Stab.* **2007**, *92* (8), 1421–1432. DOI: 10.1016/j.polymdegradstab.2007.03.023

(53) Yusof, N.; Ismail, A. F. Post Spinning and Pyrolysis Processes of Polyacrylonitrile (PAN)-Based Carbon Fiber and Activated Carbon Fiber: A Review. *J. Anal. Appl. Pyrolysis* **2012**, *93*, 1–13. DOI: 10.1016/j.jaap.2011.10.001

(54) Watt, W. Chemistry and Physics of the Conversion of Polyacrylonitrile Fibres into High-Modulus Carbon Fibres. *Elsevier Science Publishers B. V., Handbook of Composites* **1985**, *1*, 327-387.

(55) Georgiou, P.; Kyriakopoulou, E.; Zoumpoulakis, L. Performance of Novolac Resin- and Resole Resin-Based Carbon/Carbon Composites in Relation to Their Fabrication Conditions. *Polym. Int.* **2024**, *73* (8), 658–672. DOI: 10.1002/pi.6637

Appendix A

Supporting Information for SC-1008

I. Average Total Mass Values

Table A.A.1: Average initial mass and mass loss values at each temperature gradient for pure SC-1008.

	0.83 °C s^{-1}	3.03 °C s^{-1}	5.83 °C s^{-1}	11.54 °C s^{-1}	23.11 °C s^{-1}
Initial Mass	0.06379 ± 0.00199 g	0.05972 ± 0.00211 g	0.05593 ± 0.00380 g	0.05878 ± 0.00250 g	0.05879 ± 0.00029 g
Mass Loss	0.02936 ± 0.00405 g	0.02876 ± 0.00484 g	0.02751 ± 0.00180 g	0.02990 ± 0.00512 g	0.03026 ± 0.00045 g

II. Mole Fractions as a Function of Reaction Extent

The mole fraction data in **Figure A.A.1** is calculated directly after fitting the raw data with the library mass spectra. This is done to show that the temperature shift between runs is linear across all products.

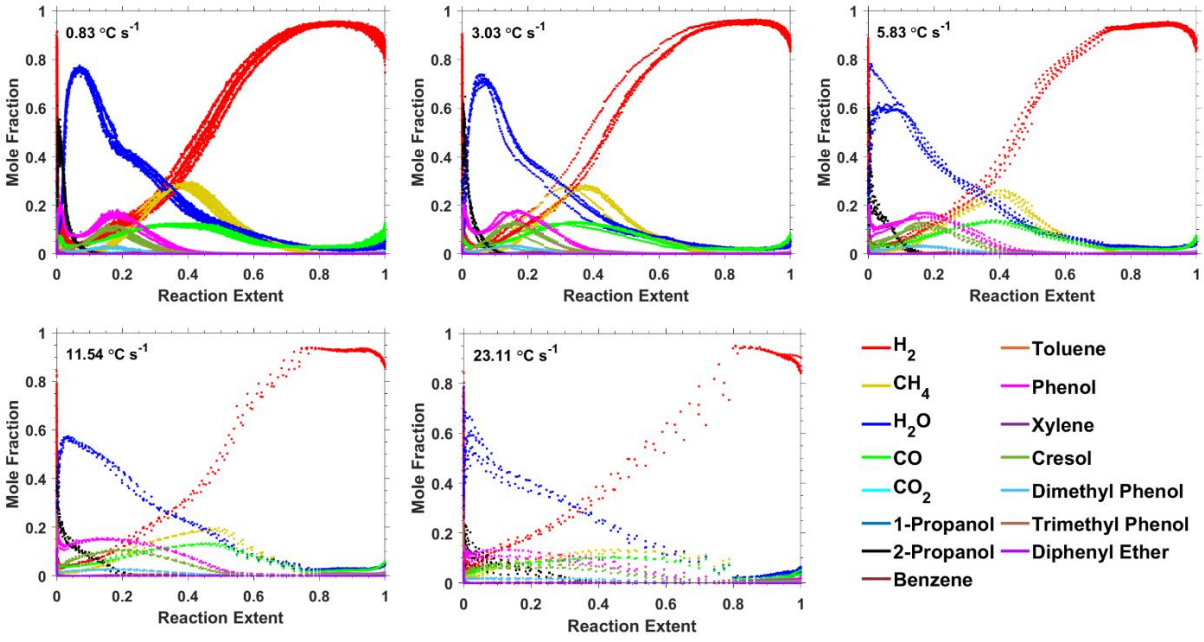

Figure A.A.1 Mole fraction as a function of reaction extent for five experimental runs at each of the five temperature gradients of 0.83 °C s^{-1}, 3.03 °C s^{-1}, 5.83 °C s^{-1}, 11.54 °C s^{-1}, and 23.11 °C s^{-1}.

The mole fraction data in **Figure A.A.2** is calculated from the molar yield fits in since it was difficult to directly fit the data shown in **Figure A.A.1**.

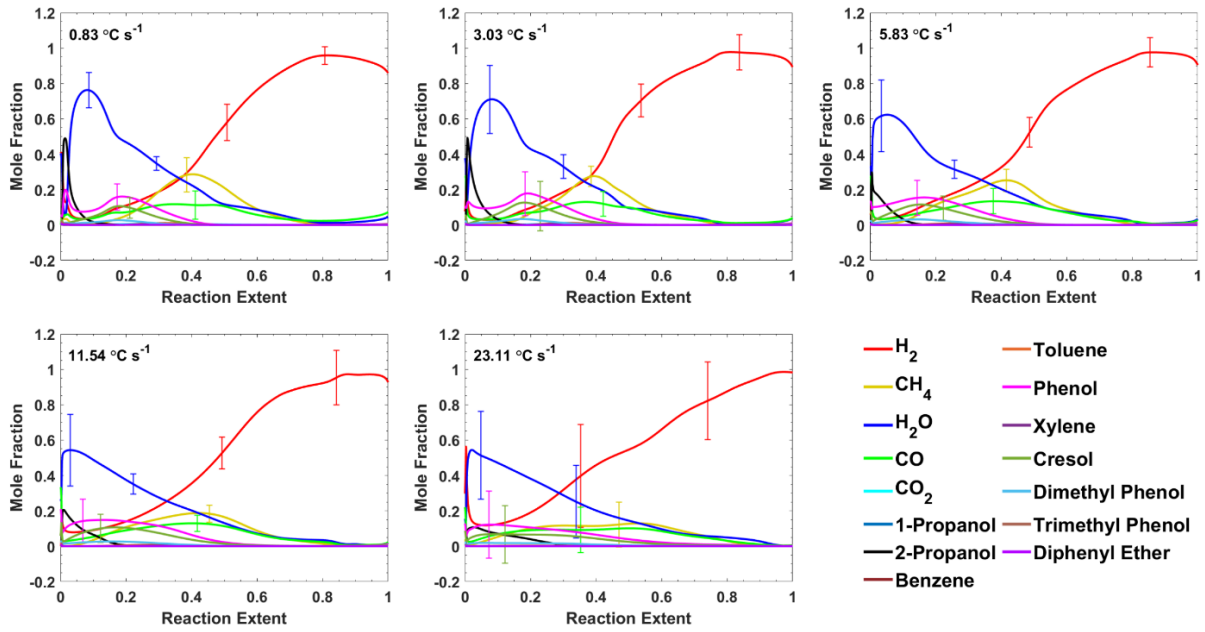

Figure A.A.2 Average fits for mole fraction as a function of reaction extent for five experimental runs at each of the five temperature gradients of 0.83 °C s^{-1}, 3.03 °C s^{-1}, 5.83 °C s^{-1}, 11.54 °C s^{-1}, and 23.11 °C s^{-1} with representative ±1σ error bars.

II. Molar Yields Plotted Without H_2 and H_2O

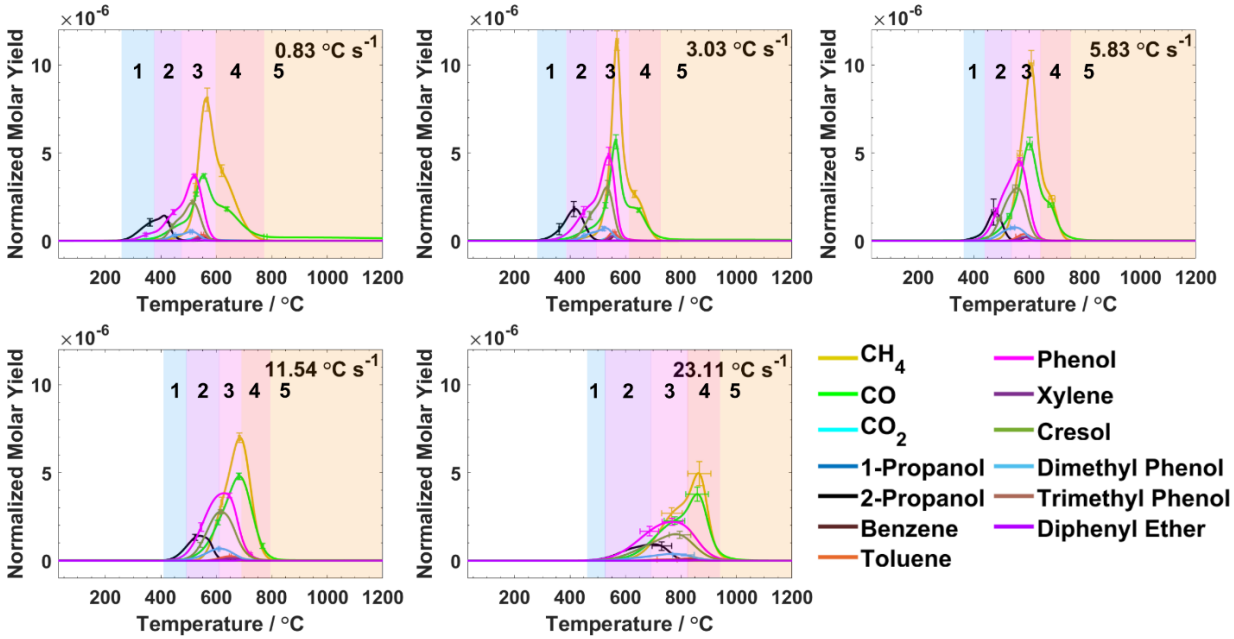

Figure A.A.3 Temperature dependence of the molar yields of each gaseous pyrolysis compound normalized to the total molar yield of 13 compounds that are assumed to evolve from pure SC-1008 during pyrolysis with five different temperature gradients, as indicated on each plot. H_2 and H_2O have been removed from the plot to expand on products with lower molar yields. Error bars represent ± 1σ for the five runs.

Appendix B

Supporting Information for PICA-D

I. Average Total Mass Values

Table A.B.1: Average initial mass and mass loss values at each temperature gradient for PICA-D.

	1.08 °C s^{-1}	3.14 °C s^{-1}	5.92 °C s^{-1}	12.55 °C s^{-1}	24.67 °C s^{-1}
Initial Mass	0.02325 ± 0.00048 g	0.02314 ± 0.00195 g	0.02430 ± 0.00125 g	0.02263 ± 0.00105 g	0.02512 ± 0.00143 g
Mass Loss	0.00417 ± 0.00024 g	0.00388 ± 0.00027 g	0.00427 ± 0.00016 g	0.00387 ± 0.00021 g	0.00378 ± 0.00024 g

II. Normalized Molar Yields Plotted Without H_2 and H_2O

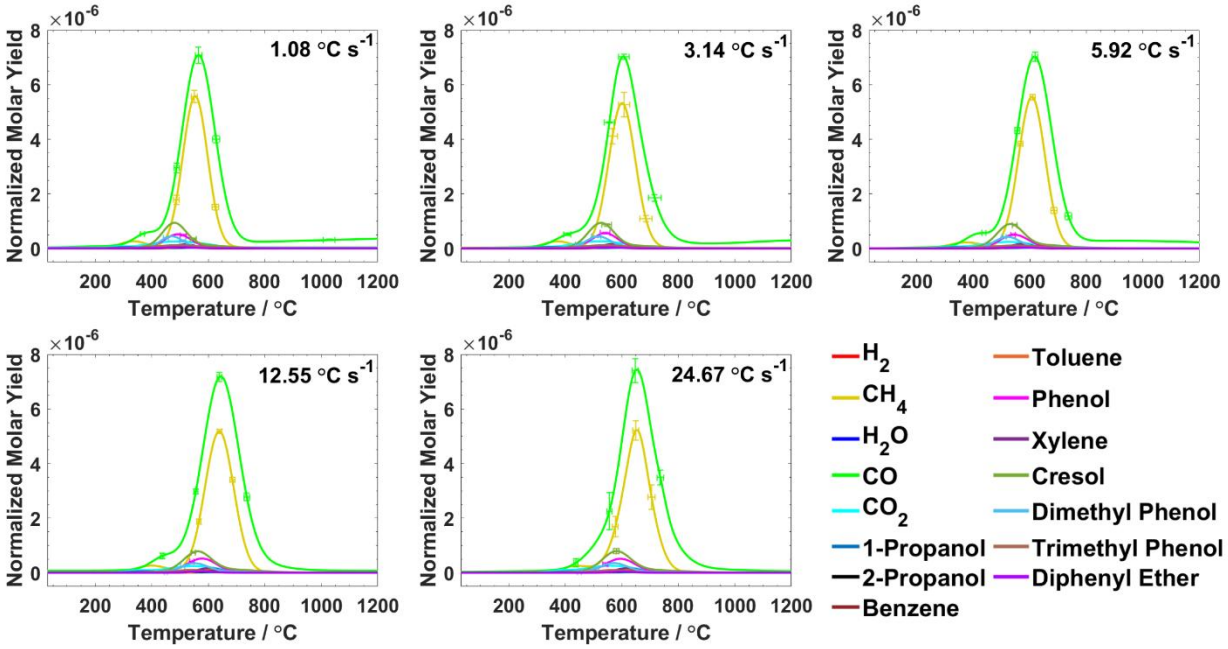

Figure A.B.1 Temperature dependence of the molar yields of each gaseous pyrolysis compound normalized to the total molar yield of 15 compounds that are assumed to evolve from PICA-D during pyrolysis with five different temperature gradients, as indicated on each plot. H_2 and H_2O have been removed from the plot and the scale has been expanded to highlight products with lower molar yields. Error bars represent ±1σ from the five pyrolysis runs.

III. Normalized Molar Yields Plotted Without H_2, H_2O, CO, and CH_4

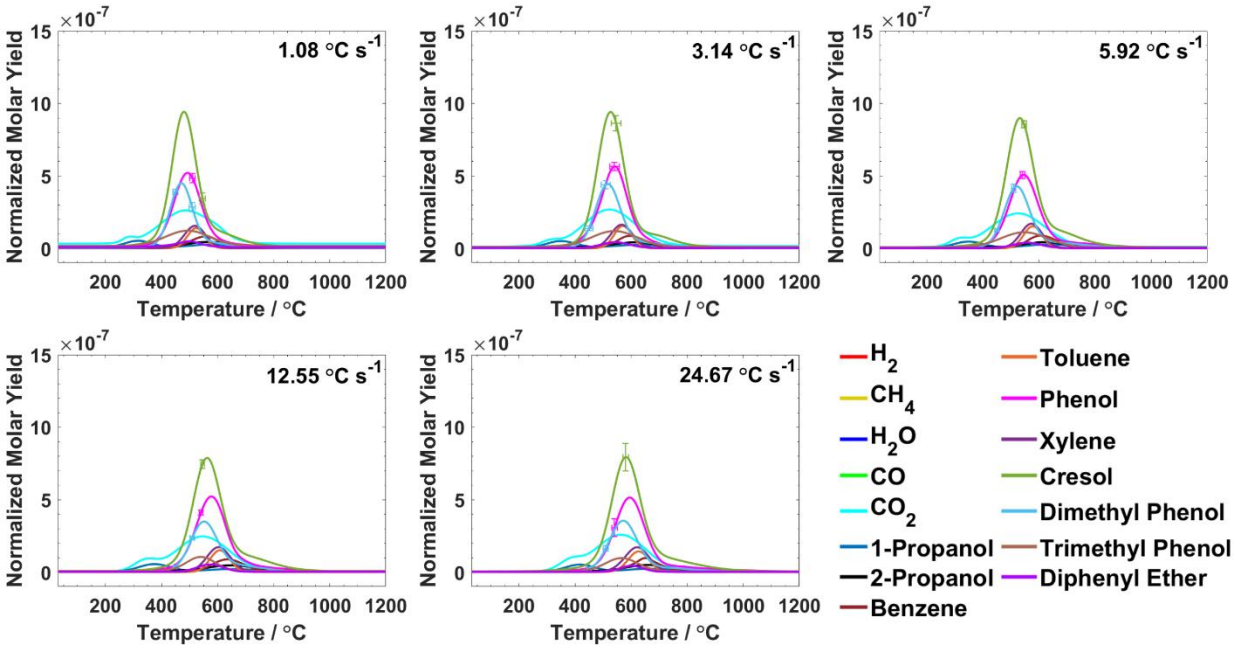

Figure A.B.2 Temperature dependence of the molar yields of each gaseous pyrolysis compound normalized to the total molar yield of 15 compounds that are assumed to evolve from PICA-D during pyrolysis with five different temperature gradients, as indicated on each plot. H_2, H_2O, CO, and CH_4 have been removed from the plot and the scale has been expanded to highlight products with lower molar yields. Error bars represent ±1σ from the five pyrolysis runs.

Appendix C

Supporting Information for 3MDCP-IL

I. Average Total Mass Values

Table A.C.1: Average initial mass and mass loss values at each temperature gradient for 3MDCP-IL.

	0.95 °C s^{-1}	2.55 °C s^{-1}	5.52 °C s^{-1}	9.59 °C s^{-1}	21.90 °C s^{-1}
Initial Mass	0.16001 ± 0.00035 g	0.16013 ± 0.00451 g	0.16933 ± 0.01905 g	0.16907 ± 0.00270 g	0.16199 ± 0.00142 g
Mass Loss	0.02906 ± 0.00042 g	0.02854 ± 0.00085 g	0.03000 ± 0.00368 g	0.03010 ± 0.00064 g	0.02945 ± 0.00032 g

II. Normalized Molar Yields Plotted Without H_2 and H_2O

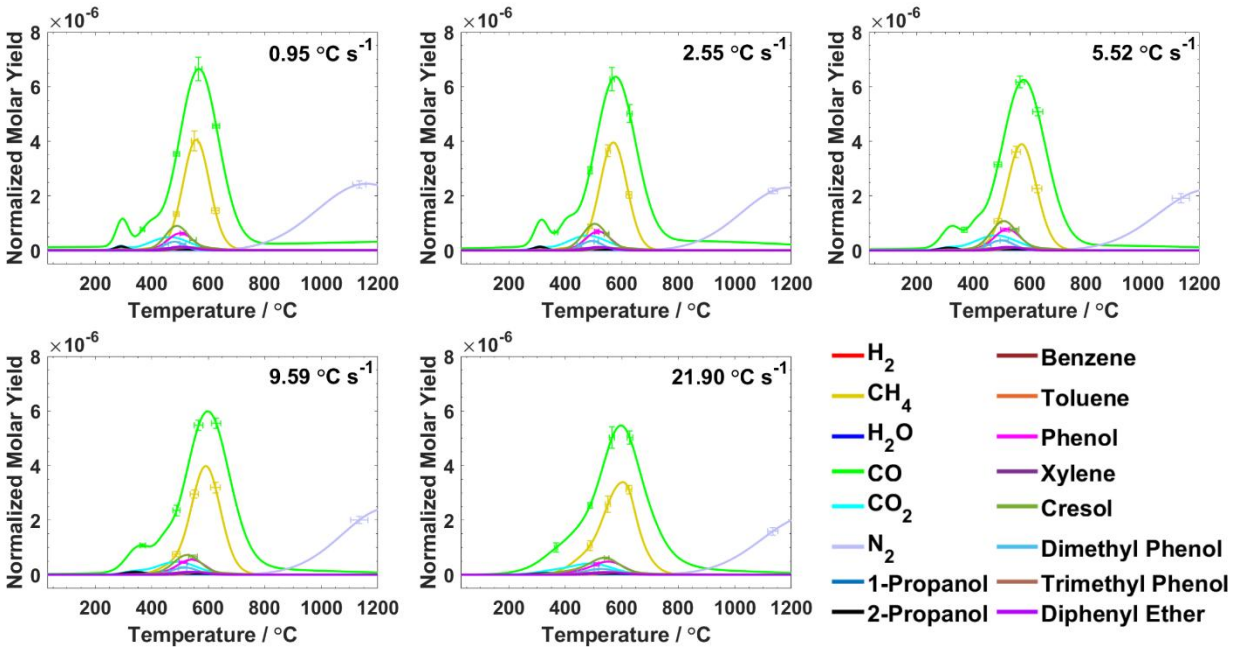

Figure A.C.1 Temperature dependence of the molar yields of each gaseous pyrolysis compound normalized to the total molar yield of 15 compounds that are assumed to evolve from 3MDCP-IL during pyrolysis with five different temperature gradients, as indicated on each plot. H_2 and H_2O have been removed from the plot and the scale has been expanded to highlight products with lower molar yields. Error bars represent ±1σ from the five pyrolysis runs.

III. Normalized Molar Yields Plotted Without H_2, H_2O, CO, and CH_4

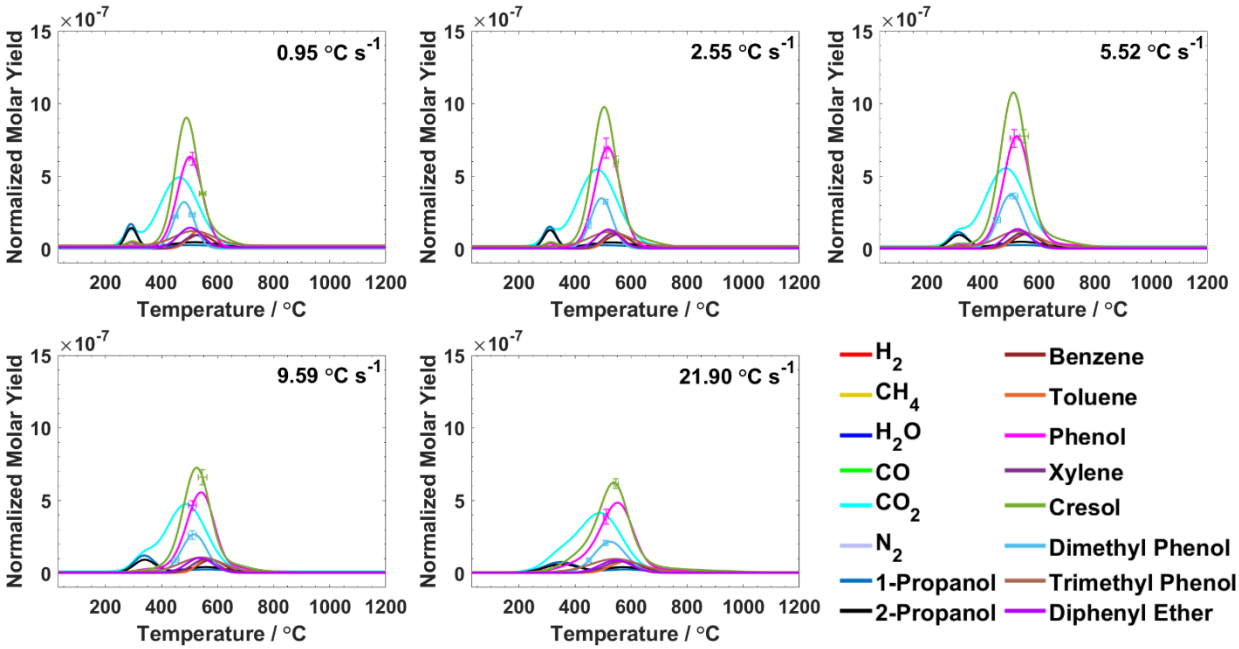

Figure A.C.2 Temperature dependence of the molar yields of each gaseous pyrolysis compound normalized to the total molar yield of 15 compounds that are assumed to evolve from 3MDCP-IL during pyrolysis with five different temperature gradients, as indicated on each plot. H_2, H_2O, CO, and CH_4 have been removed from the plot and the scale has been expanded to highlight products with lower molar yields. Error bars represent ±1σ from the five pyrolysis runs.